CHAPTER

Heavy Fermions

15

CHAPTER OUTLINE

Physics of Condensed Matter. DOI: 10.1016/B978-0-12-384954-0.00015-3

15.1 INTRODUCTION

Heavy fermions, which are also sometimes referred to as heavy electrons, are a loosely defined collection of intermetallic compounds containing lanthanide (mostly Ce, Yb) or actinide (mostly U, Np) elements. They also include other compounds such as quasi two-dimensional $CeCoIn_5$ and "Skutterdites" such as $PrOs_4Sb_{12}$. The common feature of the heavy fermions is that they have large effective mass m^* (50–1000 times greater than the mass of a free electron) below a coherence temperature T^*. The effective mass is estimated through the electronic specific heat. In general, for very low temperatures, the specific heat C of a metal can be expressed as

$$C/T = \gamma + \beta T^2, \tag{15.1}$$

where

$$\gamma = V_m k_F k_B^2 m^*/3\hbar^2. \tag{15.2}$$

Here, V_m is the molar volume, k_F is the Fermi vector, m^* is the effective mass of the electron, T is the absolute temperature, γ is the electronic contribution, and β is the contribution of the phonons to the specific heat. There is an additional spin-fluctuation term $\delta T^3 \ln T$ in the specific heat of UPt_3 and UAl_2.

For normal metals such as copper or aluminum, γ is of the order 1 mJ/mol K^2 at low temperatures. A generally accepted definition of heavy fermions is those systems that have $\gamma > 400$ mJ/f atom mol K^2 below the coherence temperature T^*. γ is generally normalized to a mole of f atoms so that there can be a comparison between systems with different structure. Some of the other properties of heavy fermions include (a) an enhanced Pauli spin susceptibility indicating a large effective mass; (b) a Wilson ratio of approximately one; (c) a huge T^2 term in the electrical resistivity; and (d) highly temperature-dependent de Haas–van Alphen oscillation amplitudes at very low temperatures. The Wilson ratio (Ref. 35) R is defined as

$$R = \frac{\pi^2 k_B^2 \chi(0)}{g^2 \mu_B^2 J(J+1)\gamma(0)}. \tag{15.3}$$

Here, $\chi(0)$ and $\gamma(0)$ are the magnetic susceptibility and specific heat at zero temperature, J is the total angular momentum, g_J is the Landé g factor, and the other symbols have their usual meanings.

$CeAl_3$, which earlier had been considered a mixed-valence compound, was the first heavy-fermion system discovered by Andres et al. in 1975. They found that below 0.2° K, $\gamma = 1620$ mJ mole/K^2 and the coefficient of the T^2 term in $\rho = AT^2$, $A = 35$ μΩ cm/K^2. The intense interest in heavy-fermion systems started with the discovery of superconductivity in $CeCu_2Si_2$ by Steglich et al.[29] in 1979. Their results are shown in Figures 15.1 and 15.2.

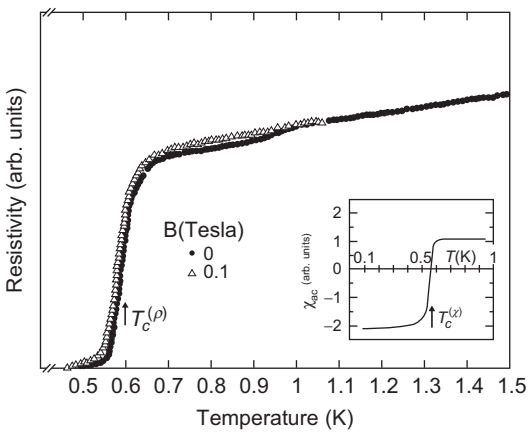

FIGURE 15.1

Resistivity (main part) and low-field ac susceptibility (inset) of $CeCu_2Si_2$ as a function of temperature. Arrows give transition temperatures $T_c^{(\rho)} = 0.60 \pm 0.03°$ K and $T_c^{(\chi)} = 0.54 \pm 0.03°$ K.

Reproduced from F. Steglich et al.[29] with permission of the American Physical Society.

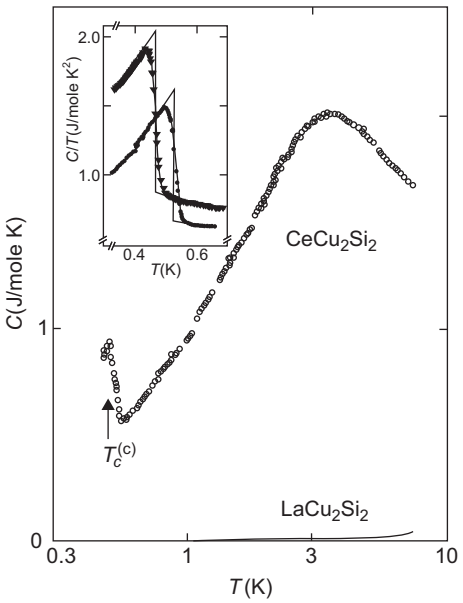

FIGURE 15.2

Molar specific heat of $CeCu_2Si_2$ as a function of temperature on a logarithmic scale. Inset shows the specific heat jumps of two other samples.

Reproduced from F. Steglich et al.[29] with the permission of the American Physical Society.

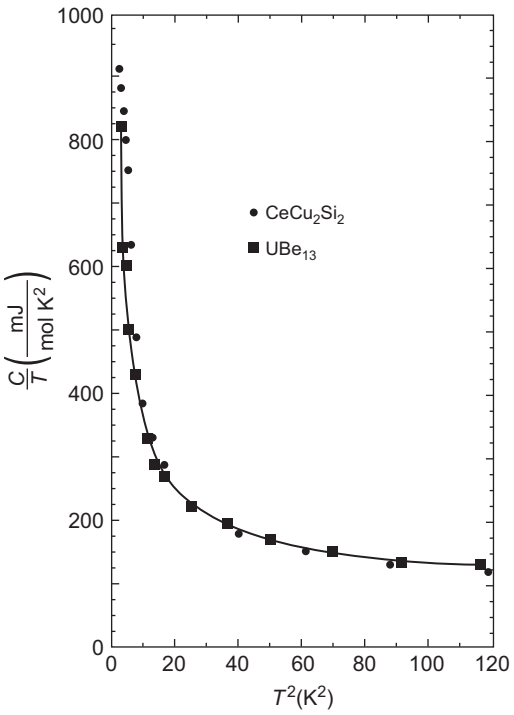

FIGURE 15.3

Specific heat of nonsuperconducting single crystals (•) and a piece of superconducting crystal (■) of UBe_{13}.

Reproduced from Stewart[30] with the permission of the American Physical Society.

The main part of Figure 15.2 shows, in a logarithmic scale, the molar specific heat of $CeCu_2Si_2$ at $B = 0$ as a function of temperature. The inset in Figure 15.2 shows in a C/T plot the specific heat-jumps of two other $CeCu_2Si_2$ samples that do not look very profound.

The specific heat-jumps below the coherence temperature T^*, which is characteristic of heavy-fermion systems, are elegantly displayed when one plots C/T versus T^2. Stewart[30] plotted C/T versus T^2 of nonsuperconducting single crystals of $CeCu_2Si_2$ and a piece of a superconducting single crystal of UBe_{13}. These results are reproduced in Figure 15.3, in which the line through UBe_{13} serves as a guide to the eye.

Since 1974, approximately 50 heavy-fermion compounds have been discovered, but there is no uniformity in their properties. For example, UBe_{13} is a superconductor in the ground state with non-Fermi-liquid properties in the normal state, whereas UPt_3 orders antiferromagnetically below the Néel temperature (T_N), exhibits a heavy Fermi-liquid state well below T_N, and has unconventional superconductivity with a multicomponent superconducting parameter. $CeAl_2$ and U_2Zn_{17} are antiferromagnets with weak moments at very low temperatures, and CeNiSn and $Ce_3Bi_4Pt_3$ are

narrow-gap semiconductors with quasiparticles having large effective masses. Some heavy-fermion superconductors such as $CeCoIn_5$ are quasi two-dimensional. The only common feature is the large effective mass below the coherence temperature and the fact that all these are highly correlated electron systems. In addition, some heavy fermions such as $CeRu_2Si_2$ exhibit metamagnetism, which has a wide variety of technological applications.

There are many factors that lead to the conclusion that the large effective mass of heavy fermions below the coherence temperature is not due to band-structure renormalization. For example, the magnitude of the nuclear relaxation rate of UBe_{13} and the ultrasonic attenuation in UPt_3 in the normal state are the same as ordinary metals. The thermal conductivity measurements in $CeCu_2Si_2$, UBe_{13}, and UPt_3 yield results similar to ordinary metals.

There have been several powerful techniques applied to discuss the theory of these strongly correlated systems. However, the theory of these systems lags behind the experiment. In this chapter, we will discuss the properties of the wide variety of these correlated systems without going into the details of the complex theories.

15.2 KONDO-LATTICE, MIXED-VALENCE, AND HEAVY FERMIONS

15.2.1 Periodic Anderson and Kondo-Lattice Models

It has been noted that the majority of the rare-earth and actinide compounds have local moments and can be classified as systems in the magnetic regime. The f orbitals have no charge fluctuation in this region and have integral valence. Therefore, they can be considered to be in a Mott insulating stage. Weak residual spin polarization of the conduction electrons, Rudderman–Kittel–Kasuya–Yosida (RKKY) interactions between the local moments (Refs. 12, 21, 36), magnetic transition at low temperatures, and spin-wave excitations occur. The spin waves scatter the conduction electrons at low temperatures.

To correlate and to study their dependence on the various relevant parameters, the simplest Hamiltonian is the orbitally nondegenerate periodic Anderson model (Ref. 1). The periodic Anderson model for a system consisting of a set of N sites is denoted by sites i, j. On each site, there are two orthogonal nondegenerate orbitals that will be referred to as C and f. The Hamiltonian is assumed to have the form

$$H = t\sum_{i\neq j,\sigma}\hat{C}^{\dagger}_{i\sigma}\hat{C}_{j\sigma} + V\sum_{i\neq j,\sigma}(\hat{C}^{\dagger}_{i\sigma}\hat{f}_{j\sigma} + \hat{f}^{\dagger}_{j\sigma}\hat{C}_{i\sigma}) + \varepsilon_f\sum_{i,\sigma}\hat{f}^{\dagger}_{i,\sigma}\hat{f}_{i\sigma} + U\sum_{i}\hat{f}^{\dagger}_{i\uparrow}\hat{f}_{i\uparrow}\hat{f}^{\dagger}_{i\downarrow}\hat{f}_{i\downarrow}. \tag{15.4}$$

Here, t (which can be positive or negative) is the transfer (hopping) integral of the extended orthogonal orbitals between sites i and j (restricted to nearest neighbors in our model). $\hat{C}^{\dagger}_{i\sigma}$ and $\hat{C}_{j\sigma}$ are the creation and annihilation operators for these extended orbitals at sites i and j with spin σ. There is one extended orbital per site per spin with a mean energy that is the origin of the energy scale. $\hat{f}^{\dagger}_{i\sigma}$ and $\hat{f}_{i\sigma}$ are the creation and annihilation operators for the localized f orbitals (i denotes the site) with energy ε_f. V is a positive hybridization parameter between the localized and the band orbitals in neighboring sites. The third term represents the single-particle energy of the isolated f orbitals. The fourth term is an interaction of the Hubbard type between electrons of the f orbitals on the same site. U is the Coulomb repulsion between two electrons of opposite spin in the f orbital and

describes a short-range interaction between them. U is positive, whereas t and ε_f can have either sign. When we consider the f orbital only on a single site, the model (Eq. 15.4) is reduced to a single-impurity Anderson model (Ref. 1), as discussed in Section 13.9, except that the localized magnetic moment for rare-earth metals is due to $s-f$ mixing instead of $s-d$ mixing as originally visualized in the single-impurity Anderson model.

The Hamiltonian (Eq. 15.4) can be augmented by additional terms such as second-neighbor hopping or Coulomb repulsion between extended orbitals and f electrons, or between electrons on different sites. Because the orbital degeneracy is neglected, there is no Hund's rule coupling between the f orbitals in this model. However important such terms are in applications to real systems, they are ignored here in the belief that they would contribute nothing really essential to the qualitative physics.

When each f orbital is occupied by a single electron (either up-spin or down-spin), the system is described as the Kondo regime. The empty sites and doubly occupied sites become virtual states. The low-energy physics of the periodic Anderson model (Eq. 15.4) can be described by an effective model where the f-electron degrees of freedom are represented by localized spins. Schrieffer and Wolff (Ref. 24) (Problem 15.1) used a second-order perturbation with respect to V to obtain an effective Hamiltonian

$$H = t\sum_{j\neq i,\sigma}(C^{\dagger}_{i\sigma}C_{j\sigma} + H.C.) + J\sum_{i} S_i \cdot S^c_i, \tag{15.5}$$

where

$$S_i = \frac{1}{2}\sum_{\sigma,\sigma'}\tau_{\sigma,\sigma'} f^{\dagger}_{i\sigma} f_{i\sigma'}, \tag{15.6}$$

$$S^c_i = \frac{1}{2}\sum_{\sigma,\sigma'}\tau_{\sigma,\sigma'} C^{\dagger}_{i\sigma} C_{i\sigma'}, \tag{15.7}$$

and τ are the Pauli spin matrices. Thus, S^c_i are the spin-density operators of the conduction electrons, and S_i are the localized spins. J is the exchange interaction, which is antiferromagnetic ($J>0$) and inversely proportional to U. Under symmetric conditions, $J = 8V^2/U$.

Thus, the rare-earth compounds that have either localized four f-electrons (Ce, Yb) or five f electrons (U, Np) can be considered as a Kondo-lattice (Ref. 9), where at each lattice site a local moment interacts via an exchange coupling J with the spin of any conduction electron sitting at the site. The Hamiltonian in Eq. (15.5) is also known as the Kondo-lattice model (Ref. 9). The exchange coupling is the source of interesting many-body effects in the Kondo-lattice model. The complexity of solving the Kondo-lattice model arises due to the complex correlation effect involving both the localized spin and the itinerant electron degrees of freedom. In fact, a conduction electron undergoes a spin-flip process with a localized spin if the spin is antiparallel. The conduction electron leaves a trace of its spin exchange processes with the localized spins while moving around the lattice. The direction of the localized spins is determined by the history of the electrons that passed through this site. Thus, the conduction electrons are no longer independent. There are similar correlation effects in the periodic Anderson model due to the dynamic aspects of the localized electrons. Because these systems are highly correlated, most of the theoretical models developed during the past 30 years are approximate treatments of the complex problem.

15.2.2 Mixed-Valence Compounds

The properties of rare-earth metals and their compounds as well as the actinide compounds have been the subject of a great deal of interest for the past 40 years. A subclass of these rare-earth and the actinide compounds is known as mixed-valence compounds, which are poor metals but have a fluctuating valence. Clear indication that two ionic valence states are present in these compounds is provided by X-ray photoelectron spectra in which the two valence states are seen side by side. They are also evident by both photoemission measurements as well as by isomer-shift measurements. In these compounds, near the Fermi energy, the s and d electrons as well as the much heavier f electrons are present. A simple explanation is that because in the ground state, both f^n and $(f^{n-1} + \text{conduction electron})$ configurations are present, their energies must be very close. The difference of energy is on the order of the hopping line width. The extra electron is assumed to go into an extended state, so its energy is equal to the Fermi energy. The extra available f orbital can be described as a localized state, with energy $\in_f$ nearly equal to the Fermi energy E_F, and that can accept one electron but not two.

The mixed-valence compounds generally form with rare-earth elements only at the beginning, the middle, and the end of the rare-earth series. The reason that the beginning and the end of the rare-earth series are favored is that a closed shell screens the nuclear charge very effectively. Hence, the $4f$ electron in Ce and the $4f$ hole in Yb are loosely bound and not far off from the $5d$ configuration. The middle of the rare-earth series is favored because of the importance of Hund's rule coupling. The final occupied f-level, even for Sm, is not far below the d-level.

A typical example of a mixed-valence compound is SmS, which is a semiconductor at normal pressure. Sm has the electronic structure [Xe] $4f^5 5d^0 6s^2$, and S has the electronic structure [Ne] $3s^2 3p^4$. In compounds, the d-level broadens into a band and hybridizes with the $6s$ band, but the f-levels are essentially unaffected. In a schematic electronic structure, one can visualize a localized f^6-level in the gap between the $5d - 6s$ band and the $s - p$ bands.

Under pressure, the lower of the crystal field split d-bands broadens and moves down in energy relative to the f-level and ultimately crosses it. When the $f - d$ gap goes to zero, a metal insulator transition occurs. The electronic structure and the density of states for the metallic state are shown schematically in Figure 15.5.

The f-levels hybridize with the d level on a neighboring atom because they cannot hybridize with the d-level of the same atom (the f^6 configuration has a total $J = 0$). The "bandwidth" of the hybridized f-band is very narrow so that in the density of states, over the smooth $s - d$ background, there is a sharp-peak attributable to the f-like atomic character in a tight-binding representation. The wave functions near this peak are linear combinations of f-like and d-like wave functions and can be written as

$$\psi_{\mathbf{k}}(\mathbf{r}) = a_{\mathbf{k}}\phi_d(\mathbf{r}) + b_{\mathbf{k}}\phi_f(\mathbf{r}), \tag{15.8}$$

where the proportion $a_{\mathbf{k}}$ to $b_{\mathbf{k}}$ varies rapidly near the peak. The f^6-level, which is nondegenerate due to correlation energy, accommodates only one electron per atom. Because this peak is derived from the f^6-level, the integrated density

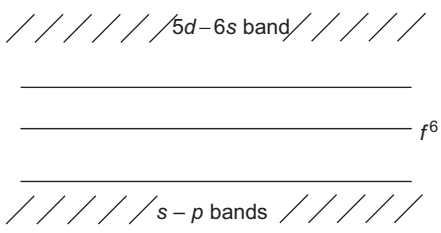

FIGURE 15.4

Schematic structure of SmS in the semiconducting phase.

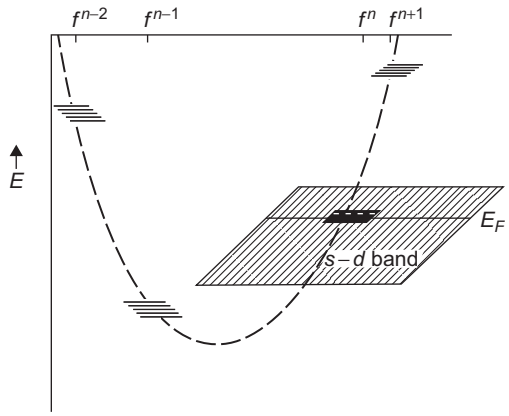

FIGURE 15.5

Electronic energy levels for mixed-valence materials. A wide *sd* band overlaps one of the configurations of the multiplet splitting of *f* electrons.

Reproduced from Varma[32] with the permission of the American Physical Society.

of states of f-like character in it is also one-electron per atom. Hence, at $T=0$, the Fermi level is pinned to lie in the f peak. This characteristic is in a sense the definition of mixed-valence compounds. The wave function in Eq. (15.8) represents the linear combination of the atomic orbital states, which is partly f^5d and partly f^6. The d electron is not affected by the local atomic exchange and correlations because it is relatively free. Thus, $\psi_{\mathbf{k}}(\mathbf{r})$ represents a linear combination of 3+ and 2+ valence states on the rare-earth ion, and the compound is known as a mixed-valence system. The average valence can be defined as

$$V_{av} = \sum_{\mathbf{k}} |a_{\mathbf{k}}|^2 / |\sum_{\mathbf{k}} |b_{\mathbf{k}}|^2, \tag{15.9}$$

where the sum is over the occupied part of the occupied band. However, the instantaneous valence V_{inst} will be different from V_{av} because the f electrons have a nonzero bandwidth.

15.2.3 Slave Boson Method

The slave boson method was developed for the $U=\infty$ periodic Anderson model that had the constraint $n_f \leq 1$ at each site. The essential feature of this method is that the localized electron operators are written as a composition of a fermion $\hat{f}$ and a boson $\hat{b}$, where we may consider the boson as an f vacancy. Every site is occupied either by an $\hat{f}$ fermion or a $\hat{b}$ boson. The localized electron operators are written as a composition of a boson $\hat{b}$ and a fermion $\hat{f}$. One defines

$$f_{i\sigma}^{\dagger} = \hat{f}_{i\sigma}^{\dagger}\hat{b}_i \quad \text{and} \quad f_{i\sigma} = \hat{b}_i^{\dagger}\hat{f}_{i\sigma}. \tag{15.10}$$

The operator equality,

$$\sum_{\sigma} \hat{f}_{i\sigma}^{\dagger}\hat{f}_{i\sigma} + \hat{b}_i^{\dagger}\hat{b}_i = 1, \tag{15.11}$$

satisfies the preceding condition. The Anderson lattice Hamiltonian can be written as

$$H = \sum_{\mathbf{k},\sigma} \varepsilon_{\mathbf{k}} c_{\mathbf{k}\sigma}^{\dagger} c_{\mathbf{k}\sigma} + \varepsilon_f \sum_{i,\sigma} \hat{f}_{i\sigma}^{\dagger}\hat{f}_{i\sigma} + V\sum_{i,\sigma}(c_{i\sigma}^{\dagger}\hat{b}_i^{\dagger}\hat{f}_{i\sigma} + \hat{f}_{i\sigma}^{\dagger}\hat{b}_i c_{i\sigma}) + \sum_i \lambda_i \left(\sum_{\sigma} \hat{f}_{i\sigma}^{\dagger} f_{i\sigma} + \hat{b}_i^{\dagger} b_i - 1\right). \tag{15.12}$$

Here, λ_i is a Lagrangian multiplier for the site i and is needed to impose the local constraints. The properties of the Hamiltonian (Eq. 15.12) are usually discussed in a mean-field approximation. It is assumed that the bosons have Bose condensations, $<\hat{b}_i> = b_0$, and the Lagrange multiplier $\lambda_i = \lambda_0$ for all sites. Thus, the constraint is obeyed only on the average over the whole system.

15.2.4 Cluster Calculations

To correlate the mixed-valence, Kondo, and heavy-fermion behavior and to study how they correspond to different regimes of one fundamental phenomenon (at least in Ce systems), Misra et al.[17] considered the application of the periodic Anderson model to finite clusters with periodic boundary conditions. Although the phrase "periodic Anderson model" is somewhat inappropriate when applied to a small system, they used it in reference to a four-atom cluster in which each site has a localized orbital and an extended orbital with appropriate Coulomb repulsion, hybridization, and transfer matrix elements. In a later paper, they extended the number of electrons to eight particles, but the results were similar. The value of small cluster calculations is that exact solutions of the Hamiltonian are obtained. However, it has to be recognized that in some respects, small clusters are not representative of bulk materials. For example, at sufficiently low temperatures the specific heat of a cluster model will vanish exponentially, and the magnetic susceptibility will either be infinity or zero. The large number of states obtained even for a small cluster suggests that statistical mechanics may give results that fairly represent a large system over a reasonable range of temperatures.

Misra et al. (Ref. 17) applied the periodic Anderson model (Eq. 15.4) to four-site tetrahedral clusters of equal length with periodic boundary conditions, thereby including the band structure effects. For example, their model Hamiltonian for a tetrahedron is identical to that of an fcc lattice if the Brillouin zone sampling is restricted to four reciprocal-lattice points, the zone center Γ, and the three square-face-center points X. They studied the region of crossover between the magnetic, Kondo, and mixed-valence regimes by varying the different parameters $U/|t|$, $V/|t|$, and $E_f/|t|$, and their results for the tetrahedron, which reflect the properties of cerium alloys, are presented in Figure 15.6.

One can distinguish the three regimes by considering n electrons per site. Consider the non-f electrons to constitute an electron reservoir. In Figure 15.6, E_d is the Fermi level when there are n non-f electrons per site, and $E_{d'}$, is the Fermi level when there are $n-1$ electrons per site (if there is no interaction with the f electrons). E_F is the chemical potential when the f electrons are in contact with the electron reservoir. Let E_f be the energy boundary such that at $T=0$, the ion will be in the f^0 state if $E_F < E_f$ and in the f^1 state if $E_F > E_f$. $E_f + U$ is another ionization boundary separating the f^1 state from the f^2 state. The crossover from one regime to another depends sensitively on the various parameters U,V, and E_f as well as on the geometry (band structure).

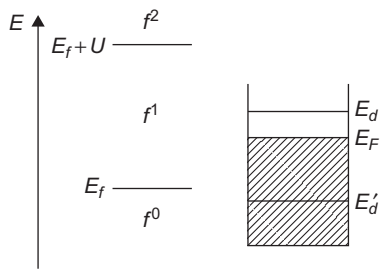

FIGURE 15.6

A schematic diagram illustrating the dependence of the three different regimes on the position of the *f*-level.

The Hamiltonian (Eq. 15.4) is conveniently considered on a basis of states diagonal in occupation numbers; Misra et al. (Ref. 17) calculated the many-body eigenstates and eigenvalues. Because spin is a good quantum number, the states can be classified as spin singlets, triplets, and quintets. For $n = 4$, there are 784 singlet, 896 triplet, and 140 quintet states. For $n = 8$ (Ref. 3), there are 12,870 states available for eight particles. These rather large numbers of states should tend to make the results somewhat representative of large systems except at extremely low temperatures (lower

than the separation between the ground state and the first excited state). The significant results are projected through the diagram in Figure 15.7.

Misra et al. (Ref. 17) constructed a computer program to diagonalize the Hamiltonian within subspaces of fixed values of S_z. They calculated the f-state occupation (n_f), temperature dependence of specific heat (C_v), and the magnetic susceptibility (χ_f) of the f electrons (by using a canonical ensemble) for a large number of parameters. In Figure 15.8, a typical example is presented by plotting C_v/T against T for E_f ranging from -5.0 to -4.0 (n_f varies from 0.9943 to 0.9788).

We notice that for $E_f = -5.0$, C_v/T increases very rapidly at very low temperatures (which mimics the onset of heavy-fermion behavior) but gradually decreases as E_f is increased until the

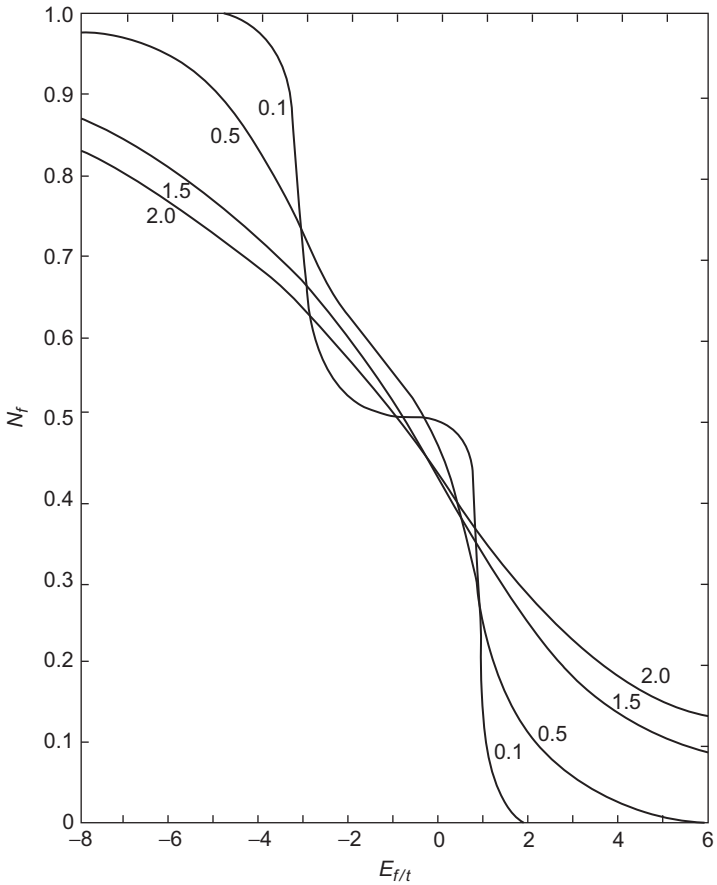

FIGURE 15.7

The f occupation number per site, n_f, in the four-electron ground state in terms of E_f and various hybridization energies V for $t = -1$, $U = 50$ for a tetrahedron.

Reproduced from Misra et al.[17] with the permission of the American Physical Society.

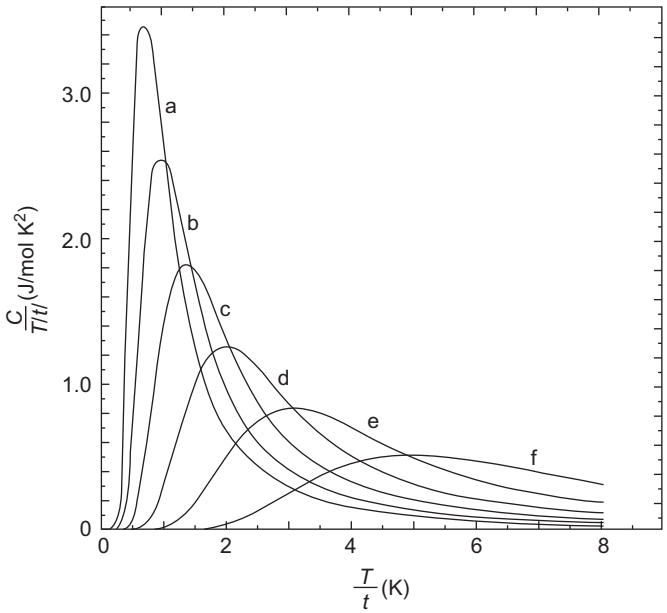

FIGURE 15.8

$Cv/T/|t|$ versus $T/|t|$ for various E_f for E negative, $U = 50$, and $V = 0.1$ for a tetrahedron. Curve (a), $E_f = -5.0$; curve (b), $E_f = -4.8$; curve (c), $E_f = -4.6$; curve (d), $E_f = -4.4$; curve (e), $E_f = -4.2$; curve (f), $E_f = -4.0$. (All parameters in units of $|t|$.)

Reproduced from Misra et al.[17] with the permission of the American Physical Society.

heavy-fermion feature has practically disappeared when $E_f = -4.2$. To explain the unusual increase in C_v/T, Misra et al. (Ref. 17) plotted the energy-level diagram (Figure 15.9) of the first few many-body states for each of these E_f as well as for $E_f = -3.0$.

In Figure 15.9, for $E_f = -5.0$, the ground state is a singlet, but the next two higher-energy states are a triplet and a quintet, which are nearly degenerate with the ground state. The low-temperature rise in C_v is determined by these three levels. As E_f increases, the separation between the lowest three levels increases, and the rise in C_v/T correspondingly decreases. Thus, the heavy-fermion behavior is obtained when the many-body ground state is a singlet but nearly degenerate to two other magnetically ordered states. The same pattern is repeated for a tetrahedron for $t = 1$, except that in some cases the ground state is a magnetically ordered triplet state. In such cases, the ground state of the heavy-fermion system would be magnetically ordered.

In Figure 15.10, Misra et al. plotted $k_B\chi_f T/(g\mu_B^2)(\equiv \chi_f T)$ versus $T/|t|$ to compare their results with the benchmark results for the single-impurity Anderson model. They defined a "frozen-impurity" regime ($\chi_f T = 0$), a free orbital regime ($\chi_f T \approx 0.125$), a valence-fluctuation regime ($\chi_f T \approx 0.167$), and a local moment regime ($\chi_f T \approx 0.25$). In addition, they defined an "intermediate regime" for which $0 < \chi_f T < 0.125$, but $\chi_f T$ essentially remains a constant in this regime.

We note from Figure 15.10 that when $E_f = -5.0$ ($n_f = 0.994$), there is a transition from the frozen-impurity to the local-moment regime. For $E_f = -3.0$ ($n_f = 0.725$), there is a transition from

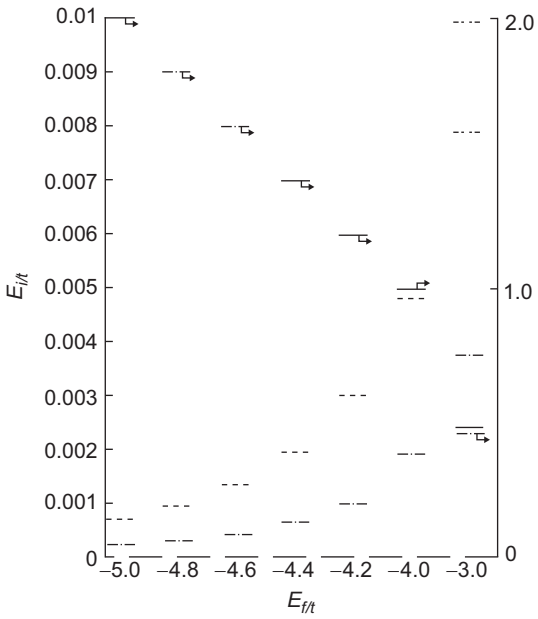

FIGURE 15.9

Energy-level diagram of the first few many-body states for various E_f for t negative, $U = 50$, $V = 0.1$ for a tetrahedron. (All parameters in units of $|t|$.)

Reproduced from Misra et al.[17] with the permission of the American Physical Society.

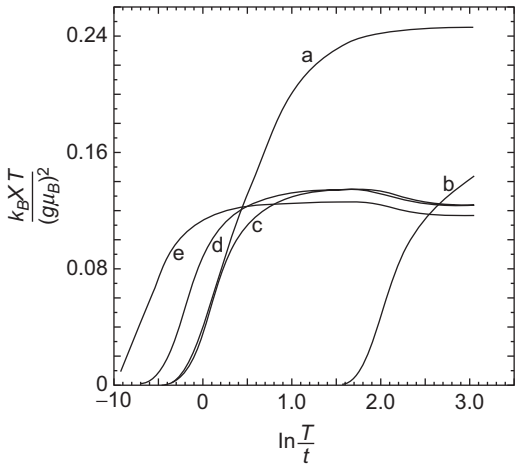

FIGURE 15.10

$k_B \chi_f T/(g\mu_b^2)$ versus $\ln T/|t|$ for $t = -1$, $U = 50$, and $V = 0.1$ for various E_f for a tetrahedron. Curve (a), $E_f = -5.0$; curve (b), $E_f = -3.0$; curve (c), $E_f = -1.0$; curve (d), $E_f = -0.5$; curve (e), $E_f = 0.5$. (All parameters in units of $|t|$.)

Reproduced from Misra et al.[17] with the permission of the American Physical Society.

the frozen-impurity to the valence-fluctuation regime. When E_f is further increased, the transition is from the frozen-impurity to the free orbital regime. The high-temperature results are in excellent agreement with the single-impurity "benchmark" results.

When we compare the specific heat curves with the χT curves for the same parameters, the specific heat maxima generally occur below the temperature at which χT reaches its high-temperature value (i.e., the crossover temperature from enhanced Pauli- to Curie-like susceptibility). The main reason is that at low temperatures where C_v is a maximum, the many-body states with magnetic moments are still just becoming thermally populated. The same broad features have also been observed experimentally.

It was generally believed that as E_f is increased from far below E_d (Figure 15.6), there would be a transition from the magnetic to the Kondo-lattice regime. However, Misra et al. (Ref. 17) found that for some choice of parameters, the system undergoes a transition from a Kondo-lattice to a magnetic regime as E_f is increased. Subsequently, it reenters a Kondo-lattice regime for higher values of E_f. This unusual feature of reentry to the Kondo-lattice regime is very sensitive to the hybridization parameter and occurs only for low $V/|t|$ values, which are the most important parameters in determining n_f as well as the thermodynamic properties.

15.3 MEAN-FIELD THEORIES

15.3.1 The Local Impurity Self-Consistent Approximation[17]

The dynamical mean-field theory is a very powerful tool for studying the strongly correlated system. In this approach, a lattice model is replaced by a single-site quantum impurity problem embedded in an effective medium determined self-consistently. This leads to an intuitive picture of the local dynamics of a quantum many-body problem. Because the impurity problem has been extensively studied, the self-consistency condition incorporates the translation invariance and the coherence effects of the lattice. This approach is now popularly known as the local impurity self-consistent approximation (LISA). The LISA freezes spatial fluctuations but includes local quantum fluctuations and is therefore characterized as a dynamical mean-field theory. The on-site quantum problem is still a many-body problem that can be addressed by using a variety of techniques. The dynamical mean-field theory becomes exact in the limit of large spatial dimensions $d \to \infty$ or in the limit of large lattice coordination.

In the mean-field theory, a lattice problem with many degrees of freedom is approximated by a single-site effective problem. The dynamics at a given site are the interaction of the degrees of freedom at this site with an external bath created by the degrees of freedom on the other sites. A simple example is an application to the Hubbard model in which the Hamiltonian is

$$H = -\sum_{<ij>,\sigma} t_{ij}(C_{i\sigma}^{\dagger}C_{j\sigma} + C_{j\sigma}^{\dagger}C_{i\sigma}) + U\sum n_{i\uparrow}n_{i\downarrow}. \tag{15.13}$$

An imaginary-time action (the local effective action) for the fermionic degrees of freedom $(C_{o\sigma}, C_{o\sigma}^{\dagger})$ at site o is

$$S_{eff} = -\int_0^{\beta} d\tau \int_0^{\beta} d\tau' \sum_{\sigma} C_{o\sigma}^{\dagger}(\tau) g_0^{-1}(\tau - \tau') C_{o\sigma}(\tau') + U\int_0^{\beta} d\tau n_{\sigma\uparrow}(\tau) n_{\sigma\downarrow}(\tau). \tag{15.14}$$

Here, $g_0(\tau - \tau')$, the generalized "Weiss function," is the effective amplitude for a fermion to be created on the isolated site at time τ (coming from the "external bath") and destroyed at time τ' (going back to the bath). Because g_0 is a function of time, it accounts for local quantum fluctuations. It can be shown that (Problem 15.2)

$$g_0(i\omega_n)^{-1} = i\omega_n + \mu + G(i\omega_n)^{-1} - R[G(i\omega_n)^{-1}]. \tag{15.15}$$

$G(i\omega_n)$, the on-site interacting Green's function, is calculated from

$$G(\tau - \tau') = -< TC(\tau)C^{\dagger}(\tau') >_{S_{eff}} \tag{15.16}$$

$$G(i\omega_n) = \int_0^{\beta} d\tau G(\tau) e^{iw_n\tau}, \omega_n \equiv \frac{(2n+1)\pi}{\beta}. \tag{15.17}$$

Here, $R(G)$ is the reciprocal function of the Hilbert transform of the density of states corresponding to the lattice. As an example, in the Hubbard model,

$$D(\varepsilon) = \sum_k \delta(\varepsilon - \varepsilon_k), \quad \varepsilon_k = \sum_{ij} t_{ij} e^{i\overrightarrow{k}\cdot\left(\overrightarrow{R_i} - \overrightarrow{R_j}\right)}. \tag{15.18}$$

The Hilbert transform $\overline{D}(\xi)$ and its reciprocal function R are defined by

$$\overline{D}(\xi) \equiv \int_{-\infty}^{\infty} d\varepsilon \frac{D(\varepsilon)}{\xi - \varepsilon}, \quad R[\overline{D}(\xi)] = \xi. \tag{15.19}$$

Eqs. (15.14) through (15.16) are the basic equations of the LISA method. However, the major difficulty lies in the solution of S_{eff}. It can be shown that solving these equations yields the local quantities, and all the $\overrightarrow{k}$ -dependent correlation functions of the original lattice Hubbard model can be obtained.

It may be noted that the LISA approach freezes spatial fluctuations but retains local quantum fluctuations. Each site undergoes transition between the four possible quantum states $|0\rangle, |\uparrow\rangle, |\downarrow\rangle, |\uparrow,\downarrow\rangle$ by exchanging electrons with the rest of the lattice or "the external bath." As an example, one can consider $(C_{o\sigma}, C^{\dagger}_{o\sigma})$ as an impurity orbital. The bath can be described as a "conduction band" described by the operators $(a_{l\sigma}, a^{\dagger}_{l\sigma})$, and the Hamiltonian is the well-known single-impurity Anderson Hamiltonian

$$H_{AM} = \sum_{l\sigma} \widetilde{\in}_l a^{\dagger}_{l\sigma} a_{l\sigma} + \sum_{l\sigma} V_l (a^{\dagger}_{l\sigma} C_{o\sigma} + C^{\dagger}_{o\sigma} a_{l\sigma}) - \mu \sum_{\sigma} C^{\dagger}_{o\sigma} C_{o\sigma} + U n_{\sigma\uparrow} n_{\sigma\downarrow}. \tag{15.20}$$

Eq. (15.20) is quadratic in $a^{\dagger}_{l\sigma}, a_{l\sigma}$, and integrating these gives rise to S_{eff} of the form given in Eq. (15.14), provided

$$g_0^{-1}(i\omega_n)^{AM} = i\omega_n + \mu - \int_{-\infty}^{\infty} d\omega \frac{\Delta(\omega)}{i\omega_n - \omega} \tag{15.21}$$

and

$$\Delta(\omega) = \sum_{l\sigma} V_l^2 \delta(\omega - \widetilde{\varepsilon}_i). \tag{15.22}$$

If the parameters $V_l, \widetilde{\varepsilon}_l$ are chosen to obtain g_0, the solution of the mean-field equations, H_{AM} becomes the Hamiltonian representation of S_{eff}. Here, $\widetilde{\varepsilon}_l$'s are effective parameters and not $\varepsilon_{\mathbf{k}}$, the single-particle energy. In addition, $\Delta(\omega)$, the conduction bath density of states, is obtained when the self-consistent problem is solved.

Thus, by using the LISA approach, one obtains the Anderson impurity embedded in a self-consistent medium from the Hubbard model. The dynamical mean-field equations are solved such that the proper g_0 is obtained. When this g_0 is inserted into the Anderson model, the resulting Green's function should obey the self-consistency condition in Eq. (15.15). The mapping onto impurity models, which have been studied by a variety of analytical and numerical techniques, is used to study the strongly correlated lattice models in large dimensions. However, it is important to solve S_{eff} by using reliable methods.

15.3.2 Application of LISA to Periodic Anderson Model

We will now briefly describe the application of the LISA method to heavy-fermion systems and the Kondo insulators (Ref. 20). This is done by using the periodic Anderson model (PAM). This model describes a band of conduction electrons that hybridize with localized $f-$ electrons at each lattice site. The PAM Hamiltonian can be written as

$$H = \sum_{\mathbf{k}\sigma} \in_{\mathbf{k}} C^{\dagger}_{\mathbf{k}\sigma} C_{\mathbf{k}\sigma} + V \sum_{i\sigma} (C^{\dagger}_{i\sigma} f_{i\sigma} + f^{\dagger}_{i\sigma} C_{i\sigma}) + \in_f \sum_{i\sigma} f^{\dagger}_{i\sigma} f_{i\sigma} + U \sum_{i} (n_{fi\uparrow} - 1/2)(n_{fi\downarrow} - 1/2), \tag{15.23}$$

where the terms were defined in Section 15.2. In the $d \to \infty$ limit, the local interaction gives rise to **k**-independent self-energy, and the various Green's functions are obtained in the form

$$\begin{aligned} G_c(i\omega_n, \mathbf{k})^{-1} &= i\omega_n - \in_{\mathbf{k}} - \frac{V^2}{i\omega_n - \in_f - \sum_f (i\omega_n)}, \\ G_f(i\omega_n, \mathbf{k})^{-1} &= i\omega_n - \in_f - \Sigma_f(i\omega_n) - \frac{V^2}{i\omega_n - \in_{\mathbf{k}}}, \\ G_{cf}(i\omega_n, \mathbf{k})^{-1} &= \frac{1}{V}\{[(i\omega_n - \in_{\mathbf{k}})(i\omega_n - \in_f - \Sigma_f(i\omega_n)] - V^2\}, \end{aligned} \tag{15.24}$$

where $\Sigma_f(i\omega_n)$ is the self-energy of the f electrons, and μ, the chemical potential, is absorbed in the definitions of $\in_{\mathbf{k}}$ and $\in_f$. It can be shown by reducing to a self-consistent single-site model that the effective action is

$$S_{eff} = -\int_0^\beta d\tau \int_0^\beta d\tau' \sum_\sigma f_\sigma^\dagger(\tau) g_0^{-1}(\tau - \tau') f_\sigma(\tau') + U \int_0^\beta d\tau [n_{f\uparrow}(\tau) - 1/2][n_{f\downarrow}(\tau) - 1/2]. \tag{15.25}$$

The f self-energy is obtained from

$$\Sigma_f = g_0 - G_f^{-1}, G_f \equiv -<Tff^\dagger>_{S_{eff}}. \tag{15.26}$$

Because the self-consistency condition requires that the Green's function of the impurity problem must be equal to the local f Green's function of the lattice model, we obtain

$$G_f(i\omega_n) = \int_{-\infty}^{\infty} \frac{d\in D(\in)}{i\omega_n - \in_f - \sum_f (i\omega_n) - V^2/(i\omega_n - \in)}. \tag{15.27}$$

Here, $D(\in)$ is the density of states (noninteracting) of the conduction electrons.

The temperature dependence of the electronic transport of the heavy-fermion systems can be calculated by using a self-consistent second-order perturbation theory in terms of the Coulomb repulsions U.

15.3.3 RKKY Interaction

There are two competing interactions in the heavy-fermion system: the indirect exchange between the moments mediated by the RKKY interaction (Refs. 12, 21, 36) and the Kondo exchange between the conduction electrons and the moments. The conducting electrons and the moments retain their identities and interact weakly. The RKKY interaction is described in the following section.

Ruderman and Kittel[21] considered the problem of nuclear-spin ordering in a metal and used second-order perturbation theory to derive an expression for the indirect nuclear spin–spin interaction (Problem 15.5),

$$H_{\text{RKKY}} = -\frac{9\pi}{8} n_c^2 \frac{J^2}{\varepsilon_F} \sum_{<ij>} \frac{\mathbf{S}_i \cdot \mathbf{S}_j}{r_{ij}^3} \left[2k_F \cos(2k_F r_{ij}) - \frac{\sin(2k_F r_{ij})}{r_{ij}} \right], \tag{15.28}$$

where k_F is the Fermi wave vector, and n_c is the density of conduction electrons. The spin–spin interaction is long ranged and changes its sign depending on the distance between the pair of spins. Kasuya discussed the magnetic properties of rare-earth metals based on Eq. (15.28).[12] Yosida[36]

showed that the oscillatory behavior originates from the Friedel oscillation of the spin polarization of conduction electrons induced by a localized spin. Therefore, Eq. (15.28) is known as the RKKY interaction.

For rare-earth metals, the Fourier transform of the RKKY interaction is given by $\chi(\mathbf{q})$, the susceptibility of the conduction electrons for wave number $\mathbf{q}$. The ground state is usually ferromagnetic if $\chi(\mathbf{q})$ is maximum at $\mathbf{q}=0$. If the maximum of $\chi(\mathbf{q})$ occurs at $\mathbf{q}=\mathbf{Q}$, the antiferromagnetic wave vector, the ground state becomes antiferromagnetic. The ground state may have a spiral spin ordering if $\chi(\mathbf{q})$ becomes maximum at a general wave vector. The Kondo effect is suppressed whenever there is any type of magnetic ordering. The low-energy physics of the Kondo effect is given by the Kondo temperature

$$T_K = \varepsilon_F e^{-1/J\rho(\varepsilon_F)}. \tag{15.29}$$

However, the characteristic energy of the RKKY interaction is given by J^2/ε_F. This energy dominates over the Kondo temperature in the weak-coupling regime.

In the strong-coupling regime, the local moments are quenched because of the formation of local singlets. The Kondo effect or the effect of singlet formation is not considered for the derivation of the RKKY interaction. The relation between RKKY interaction and the Kondo effect depends on the conduction electron density, dimensionality, and the exchange coupling. As an example, we consider two localized spins, $\mathbf{S}_1$ and $\mathbf{S}_2$. The direct exchange coupling between the two spins can be expressed as

$$H = J_{\mathrm{RKKY}}\mathbf{S}_1 \cdot \mathbf{S}_2, \tag{15.30}$$

where J_{RKKY}, the intersite coupling constant, is arbitrary. For $J>0$, the Kondo coupling is antiferromagnetic, and the ground state is a singlet. When $J > J_{\mathrm{RKKY}}$, each of the two localized spins forms a singlet with conduction electrons, and hence, the interaction between the singlets is weak. When $J_{\mathrm{RKKY}} \gg J$, the two localized spins form a singlet by themselves, and J is no longer important. There is a difference among theorists as to whether the change between the two regimes is smooth or sharp.

15.3.4 Extended Dynamical Mean-Field Theory[16]

The extended dynamical mean-field theory (EDMFT), which is an extension of DMFT, is particularly suitable to solve problems such as the competition between the exchange interaction and kinetic energy. In the EDMFT, the local quantum fluctuations are treated on the same level as the intersite quantum fluctuations. This is achieved by reducing the correlated lattice problem to a novel effective impurity problem corresponding to an Anderson impurity model with additional self-consistent bosonic baths. These bosonic baths reflect the influence of the rest of the lattice on the impurity site. As an example, they represent the fluctuating magnetic fields induced by the intersite spin-exchange interactions in the magnetic case. The intersite quantum fluctuations are included through self-consistency.

Smith and Si[28] applied the EDMFT method to the two-band Kondo-lattice model

$$H = \sum_{<ij>,\sigma} t_{ij} C^{\dagger}_{i\sigma} C_{j\sigma} + \sum_i J_K \overrightarrow{S_i} \cdot \overrightarrow{s_{c_i}} - \sum_{<ij>} J_{ij} \overrightarrow{S_i} \cdot \overrightarrow{S_j}, \tag{15.31}$$

where $\vec{S_i}$ is the impurity spin at site i, and $\vec{s_{ci}}$ is the spin of conduction $(c-)$ electrons at site i, t_{ij} is the hopping integral, and J_{ij} is the spin-exchange interaction. In the large D (dimension) limit, with $t_0 = t_{ij}\sqrt{D}$ and $J_0 = J_{ij}\sqrt{D}$, they derived an expression for the impurity action

$$S^{MF} = S_{top} + \int_0^\beta d\tau J_K \vec{S_i}\cdot\vec{s_c} - \int_0^\beta d\tau \int_0^\beta d\tau' \left[\sum_\sigma C_\sigma^\dagger(\tau) G_0^{-1}(\tau-\tau') C_\sigma(\tau') + \vec{S}(\tau)\cdot\chi_{s,0}^{-1}(\tau-\tau')\vec{S}(\tau')\right], \tag{15.32}$$

where S_{top} is the Berry phase of the impurity spin. The Weiss fields G_0^{-1} and $\chi_{s,0}^{-1}$ are determined by the self-consistency equations,

$$G_0^{-1}(i\omega_n) = i\omega_n + \mu - \sum_{ij} t_{i0}t_{0j}[G_{ij}(i\omega_n) - G_{i0}(i\omega_n)G_{0j}(i\omega_n)/G_{loc}(i\omega_n)] \tag{15.33}$$

and

$$\chi_{s,0}^{-1} = \sum_{ij} J_{i0}J_{0j}(\chi_{s,ij} - \chi_{s,i0}\chi_{s,0j}/\chi_{s,loc}). \tag{15.34}$$

Here, χ_s is the spin susceptibility. Smith and Si (Ref. 28) also showed that the effective action can be written in terms of the impurity problem,

$$\begin{aligned} H_{imp} = &\sum_{k\sigma} E_k \eta_{k\sigma}^\dagger \eta_{k\sigma} + \sum_q w_q \vec{\phi}_q^\dagger \cdot \vec{\phi}_q - \mu\sum_\sigma C_\sigma^\dagger C_\sigma \\ &+ t\sum_{k\sigma}(C_\sigma^\dagger \eta_{k\sigma} + H.C.) + J_K \vec{S}\cdot\vec{s_c} + g\sum_q \vec{S}\cdot(\vec{\phi}_q + \vec{\phi}_{-q}^\dagger), \end{aligned} \tag{15.35}$$

where E_k, t, w_q, and g are determined from the Weiss fields G_0^{-1} and $\chi_{s,0}^{-1}$ specified by

$$i\omega_n + \mu - t^2\sum_k 1/(iw_n - E_k) = G_0^{-1}(i\omega_n) \tag{15.36}$$

and

$$g^2\sum_q w_q/[(i\nu_n)^2 - w_q^2] = \chi_{s,0}^{-1}(i\nu_n). \tag{15.37}$$

15.4 FERMI-LIQUID MODELS

15.4.1 Heavy Fermi Liquids

A number of universal features are associated with the coherent Fermi-liquid state in heavy-fermion systems. They can be summarized as follows:

a. The dimensionless Wilson ratio (Ref. 35)

$$R = \frac{\chi(0)/g_J^2 J(J+1)\mu_B^2}{\gamma(0)/\pi^2 k_B^2}$$

is close to the value of unity.

b. The specific heat C_V has a rapid downturn with increasing temperature, which has been fit to a function of the form $T^3 \ln T$.

c. The resistivity ρ is proportional to T^2.

d. The low-T susceptibility χ_T also appears to vary as T^2.

In addition, the evidence of universal behavior of heavy fermions is the observation of Kadowaki and Woods that $\rho/T^2 \equiv A$ is the same multiple of γ^2 for essentially all materials.[11]

A large number of the heavy-fermion systems become heavy Fermi liquids at low temperatures in the sense that Landau's Fermi-liquid theory is still adequate to describe the physics, provided the large effective mass is included. In the Fermi-liquid theory, the specific-heat enhancement C_v/C_{v0} is related, at low temperatures, to the quasiparticle density of states at the Fermi surface. This is equivalent to an average Fermi velocity or to that of an average mass. In view of the above, the effective mass is defined as

$$\frac{C_v}{C_{v0}} = \frac{m^*}{m}. \tag{15.38}$$

Here, it is important to comment on the physical interpretation of the quasiparticles. The f electrons are supposed to be hopping from site to site. There are a large number of f electrons, and the Luttinger theorem (described later) requires the Fermi surface to contain the total number of states and not a volume containing the mobile holes in the f-band. The f electrons have very large mass due to the weak effective hybridization. Thus, the quasiparticles are essentially f electrons, and the quasiparticle bands are f-bands that have moved up to the Fermi energy and have been narrowed by correlation. The heavy Fermi liquid arises due to the Kondo screening of the localized moments at each lattice site. In a sense, the localized moments "dissolve" into the Fermi sea.

We will now summarize the concepts of the various heavy Fermi-liquid models by following the elegant but brief review of Senthil et al.[25] The Kondo-lattice model can be written as

$$H_K = \sum_{\mathbf{k}} \varepsilon_{\mathbf{k}} C^{\dagger}_{\mathbf{k}\alpha} C_{\mathbf{k}\alpha} + \frac{J_K}{2} \sum_r \mathbf{S}_r \cdot C^{\dagger}_{r\alpha} \sigma_{\alpha\alpha'} C_{r\alpha'}. \tag{15.39}$$

Here, n_c is the density of conduction electrons with dispersion $\varepsilon_{\mathbf{k}}$, $C^{\dagger}_{\mathbf{k}\alpha}$ and $C_{\mathbf{k}\alpha}$ are the creation and annihilation operators of conduction states, $\mathbf{k}$ is the momentum, and $\alpha = \uparrow, \downarrow$ is a spin index. The conduction electrons interact with f electron spins $\mathbf{S}_r$ via the antiferromagnetic Kondo exchange coupling constant J_K. Here, r is a lattice position, and $\boldsymbol{\sigma}$ are the Pauli spin matrices.

In the heavy-fermion liquid models, the charge of the $f_{r\alpha}$ electrons is fully localized on the rare-earth sites. These electrons occupy a flat dispersionless band, as shown in Figure 15.11a. Because this band is half filled, it is placed at the Fermi level. The $C_{r\alpha}$ electrons occupy their own conduction band. The Kondo exchange turns on a small hybridization between these two bands. The hybridization can be represented by a bosonic operator

$$b_r \sim \sum_{\alpha} C^{\dagger}_{r\alpha} f_{r\alpha}. \tag{15.40}$$

Because $<b_r>$ is nonzero, renormalized bands are formed (Figure 15.11b) due to the mixture of the two bands.

Because the f-band was initially dispersionless, the renormalized bands do not overlap. One now applies the Fermi-surface sum rule by Luttinger (Ref. 13), also known as the Luttinger theorem (Ref. 14). According to Luttinger, the volume enclosed by the Fermi surface is entirely determined by only the electron density. The volume is independent of the type and strength of an interaction, if the system remains a Fermi liquid and no phase transition occurs. Using this theorem leads to the conclusion that the occupied states are entirely within the lower band, and a single Fermi surface is obtained within wave vector k_F. The volume within k_F is obtained by the total density of f and c electrons.

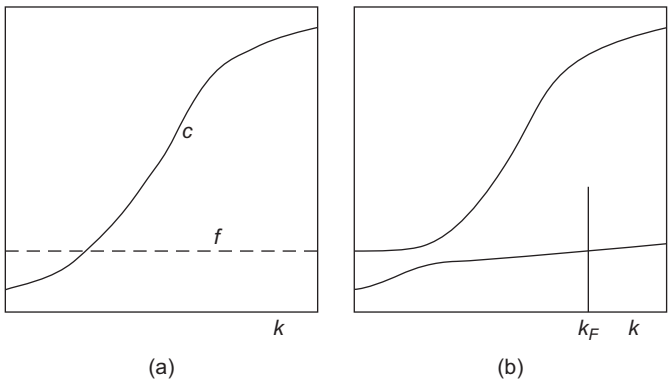

FIGURE 15.11

A completely flat *f* electron "band"—the dashed line in (a)—mixes with the conduction electrons to obtain the renormalized bands in (b). The single Fermi surface at k_F in the Fermi-liquid state contains states of which the wave number equals the sum of the *c* and *f* electrons.

Reproduced from Senthil, Sachdev, and Vojta[25] with the permission of Elsevier.

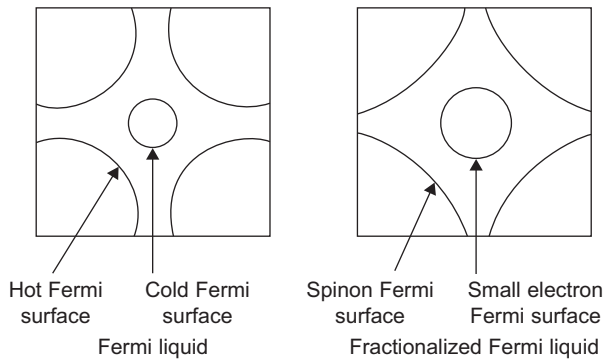

FIGURE 15.12

Fermi-surface evolution from *FL* to FL^*: The *FL* phase has two Fermi-surface sheets (the cold *c* and the hot *f* sheets) close to the transition. The *f* sheet becomes the spinon Fermi surface while the *c* sheet is the small conduction-electron Fermi surface on the FL^* side.

Reproduced from Senthil, Vojta, and Sachdev[27] with the permission of the American Physical Society.

The Fermi surface is in a region (Figure 15.11b) where the electrons primarily have an *f* character, and the band is flat. According to this model, this accounts for the large effective mass of the fermionic quasiparticles.

Because the charge fluctuations are quenched at the *f* electron sites, every rare-earth site has a constraint

$$\sum_{\alpha} f_{r\alpha}^{\dagger} f_{r\alpha} = 1, \tag{15.41}$$

which is obeyed at each rare-earth site. This implies that the theory is invariant under the space-time-dependent $U(1)$ gauge transformation

$$f_{r\alpha}^{\dagger} \rightarrow f_{r\alpha} e^{i\phi_r(\tau)}, \tag{15.42}$$

where τ is imaginary time.

15.4.2 Fractionalized Fermi Liquids

Senthil et al.[26,27] showed the existence of nonmagnetic translation-invariant small-Fermi-surface states, originally with a focus on two-dimensional Kondo lattices. These states are obtained when a local-moment system settles into a fractionalized spin liquid (FL^*) due to intermoment interactions. A weak Kondo coupling to conduction electrons leaves a sharp (but small) Fermi surface of quasiparticles (FL) of which the volume counts the conduction density, but the structure of the spin liquid is undisturbed. These states have fractionalized excitations that coexist with conventional Fermi-liquid-like quasiparticles.

In this paper, Senthil et al. considered a three-dimensional lattice by using $U(1)$ states. They focused on a three-dimensional $U(1)$ spin-liquid state with fermionic spinons that form a Fermi surface. The $U(1)$ spin-liquid state is stable to a weak Kondo coupling to conduction electrons. The $U(1)FL^*$ state consists of a spinon Fermi surface coexisting with a separate Fermi surface of conduction electrons. Senthil et al. used a mean-field theory to describe a $U(1)FL^*$ state and its transition to a heavy FL. They considered a three-dimensional Kondo–Heisenberg model on a cubic lattice,

$$H = \sum_{k} \in_{\mathbf{k}} C_{\mathbf{k}\alpha}^{\dagger} C_{\mathbf{k}\alpha} + \frac{J_K}{2} \sum_{r} \overrightarrow{S}_r \cdot C_{r\alpha}^{\dagger} \overrightarrow{\sigma}_{\alpha\alpha'} C_{r\alpha'} + J_H \sum_{<rr'>} \overrightarrow{S}_r \cdot \overrightarrow{S}_{r'}. \tag{15.43}$$

Here, $C_{\mathbf{k}\alpha}$ is the conduction electron destruction operator, $\overrightarrow{S}_r$ are the spin-1/2 local moments, and summation over repeated spin indices α is implied. In a fermionic "slave-particle" representation of the local moments

$$\overrightarrow{S}_r = 1/2 f_{r\alpha}^{\dagger} \overrightarrow{\sigma}_{\alpha\alpha'} f_{r\alpha'}, \tag{15.44}$$

where $f_{r\alpha}$ is a spinful fermion destruction operator at site r. The decoupling of the Kondo and the Heisenberg exchange is made using two auxiliary fields by a saddle-point approximation, and the mean-field Hamiltonian is

$$H_{mf} = \sum_{\mathbf{k}} \in_{\mathbf{k}} C_{\mathbf{k}\alpha}^{\dagger} C_{\mathbf{k}\alpha} - \chi_0 \sum_{<rr'>} (f_{r\alpha}^{\dagger} f_{r'\alpha} + H.C.) + \mu_f \sum_{r} f_{r\alpha}^{\dagger} f_{r\alpha} - b_0 \sum_{\mathbf{k}} (C_{\mathbf{k}\alpha}^{\dagger} f_{\mathbf{k}\alpha} + H.C.). \tag{15.45}$$

Here, b_0 and χ_0 are assumed to be real, and additional constants to H are dropped. The mean-field parameters b_0, χ_0, and μ_f are obtained from (Problem 15.3)

$$1 = <f_{r\alpha}^{\dagger} f_{r\alpha}>, \tag{15.46}$$

$$b_0 = J_K/2 <C_{r\alpha}^{\dagger} f_{r\alpha}>, \tag{15.47}$$

$$\chi_0 = J_H/2 <f_{r\alpha}^{\dagger} f_{r'\alpha}>, \tag{15.48}$$

where r and r' are nearest neighbors. At zero temperature, in the Fermi-liquid (FL) phase, χ_0, b_0, and μ_0 are nonzero. In the FL^* phase, $b_0 = \mu_0 = 0$ but $\chi_0 \neq 0$. In this state, the conduction electrons are decoupled from the local moments and form a small Fermi surface. The local-moment system is described as a spin fluid with a Fermi surface of neutral spinons.

The mean-field is diagonalized by the transformation (Problem 15.4),

$$C_{\mathbf{k}\alpha} = u_{\mathbf{k}}\gamma_{\mathbf{k}\alpha+} + v_{\mathbf{k}}\gamma_{\mathbf{k}\alpha-} \tag{15.49}$$

and

$$f_{\mathbf{k}\alpha} = v_{\mathbf{k}}\gamma_{\mathbf{k}\alpha+} - u_{\mathbf{k}}\gamma_{\mathbf{k}\alpha-}. \tag{15.50}$$

The Hamiltonian can be written in terms of the new fermionic operators $\gamma_{\mathbf{k}\alpha\pm}$,

$$H_{mf} = \sum_{\mathbf{k}\alpha} E_{\mathbf{k}+}\gamma^{\dagger}_{\mathbf{k}\alpha+}\gamma_{\mathbf{k}\alpha+} + E_{\mathbf{k}-}\gamma^{\dagger}_{\mathbf{k}\alpha-}\gamma_{\mathbf{k}\alpha-}, \tag{15.51}$$

where

$$E_{\mathbf{k}\pm} = \frac{\in_{\mathbf{k}} + \in_{\mathbf{k}f}}{2} \pm \sqrt{\left(\frac{\in_{\mathbf{k}} - \in_{\mathbf{k}f}}{2}\right)^2 + b_0^2}. \tag{15.52}$$

Here, $\in_{\mathbf{k}f} = \mu_f - \chi_0 \sum_{a=1,2,3} \cos(k_a)$. The $u_{\mathbf{k}}, v_{\mathbf{k}}$ are determined by

$$u_{\mathbf{k}} = -\frac{b_0 v_{\mathbf{k}}}{E_{\mathbf{k}+} - \in_{\mathbf{k}}}, \quad u_{\mathbf{k}}^2 + v_{\mathbf{k}}^2 = 1. \tag{15.53}$$

For the FL^* phase, $b_0 = \mu_0 = 0$ but $\chi_0 \neq 0$. The conduction-electron dispersion $\in_k$ determines the electron Fermi surface and is small. The spinon Fermi surface encloses one spinon per site and has volume half that of the Brillouin zone. Senthil *et al.* assumed that the conduction–electron filling is less than half, and the electron Fermi surface does not intersect the spinon Fermi surface. In the FL phase near the transition (small b_0), there are two bands corresponding to $E_{\mathbf{k}\pm}$: one derives from the c electrons with f character (c-band), whereas the other derives from the f particles with weak c character (f-band).

As shown in Figure 15.12, for small b_0, the Fermi surface consists of two sheets because both bands intersect the Fermi energy. The total volume is large because it includes both local moments and conduction electrons. When b_0 decreases to zero, the transition moves to FL^*, the c-Fermi surface expands in size to match onto the small Fermi surface of FL^*, and the f-Fermi surface shrinks to match onto the spinon Fermi surface of FL^*.

15.5 METAMAGNETISM IN HEAVY FERMIONS

The name *metamagnetism* was originally introduced for antiferromagnetic (AF) materials where, at low temperatures, for a critical value of the magnetic field (H), the spin flips, which gives rise to a first-order phase transition. This was extended to paramagnetic (Pa) systems where field reentrant ferromagnetism (F) would appear in itinerant magnetism. Eventually, it was used to describe a crossover inside a persistent paramagnetic state between low-field Pa phase and an enhanced paramagnetic polarized (PP) phase.

In heavy-fermion systems, the f electrons are located near the border between itinerant and local moment behavior, as shown in the phase diagram in Figure 15.13. Doniach considered a one-dimensional analog of a system of conduction electrons exchange-coupled to a localized spin in each cell of a lattice.[6] He suggested that a second-order transition from an antiferromagnetic to a Kondo spin-compensated ground state would occur as the exchange coupling constant J increased to a critical value J_c. For J near to, and slightly smaller than J_c, there would exist antiferromagnets with very weak, "nearly quenched" moments, even though the f electrons are in a state with a well-defined local nonzero spin state. The existence of this transition can be understood by comparing the binding energy of the Kondo singlet

$$W_K \sim N(0)^{-1} e^{-1/N(0)J}, \tag{15.54}$$

with that of an RKKY antiferromagnetic state

$$W_{AF} \sim CJ^2 N(0), \tag{15.55}$$

where $N(0)$ is the density of conduction electron state, and C is a dimensionless constant that depends on the band structure. As shown in Figure 15.13, for $JN(0)$ less than a critical value, the RKKY state dominates, whereas above this, the Kondo singlet binding dominates. The RKKY binding again takes over at large J, but the weak coupling formula (Eq. 15.54) breaks down in this regime.

The heavy fermions that exhibit metamagnetism are $CeRu_2Si_2$, $Sr_3Ru_2O_7$, $CeCu_{6-x}Au_x$, UPt_3, UPd_2Al_3, URu_2Si_2, $CePd_2Si_2$, $YbRh_2Si_2$, and $CeIr_3Si_2$.

There have been many theories proposed for metamagnetism of heavy fermions, but no satisfactory model is yet available. A review of the various theoretical models was made by Misra.[16]

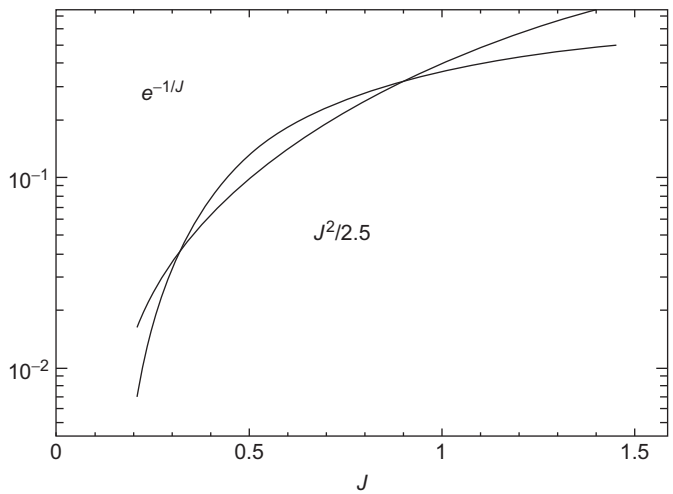

FIGURE 15.13

Comparison of *AF* with Kondo energies.

Reproduced from Doniach[6] with the permission of Elsevier.

15.6 CE- AND U-BASED SUPERCONDUCTING COMPOUNDS[16]

15.6.1 Ce-Based Compounds

Since 1979, approximately 25 unconventional superconductors have been discovered in heavy-fermion systems. Although most of these systems are Ce- and U-based compounds, a few others are quasi-two-dimensional in nature and filled skutterdites. The multiphase diagrams in UPt_3 and $U(Be_{1-x}Th_x)_{13}$ indicate unusual superconductivity with multicomponents. In fact, UPt_3 is the first odd-parity superconductor to be discovered in heavy-fermion systems. UPd_2Al_3 and UNi_2Al_3 are unconventional superconductors coexisting with the AF phase and are considered to have even- and odd-parity pairing states, respectively. There is coexistence of hidden-order and unconventional superconductivity in URu_2Si_2. UPt_3, URu_2Si_2, UNi_2Al_3, and UPd_2Al_3 have the following common features: (a) they order antiferromagnetically below T_N, ranging from 5 to 17° K; and (b) they exhibit, well below T_N and coexisting with AF order, a heavy Landau Fermi-Liquid (LFL) state that becomes unstable against a superconducting transition at T_c (ranging between 0.5 and 2° K).

Recently, a variety of heavy-fermion Ce-based superconductors were discovered due to progress in experiments under pressure. They include $CeCu_2Ge_2$, $CePd_2Si_2$, $CeRh_2Si_2$, $CeNi_2Ge_2$, and $CeIn_3$. These materials, which have the same $ThCr_2Si_2$-type crystal structure as $CeCu_2Si_2$ (except $CeIn_3$), are AF metals at ambient pressure, whereas under high pressures, the AF phases abruptly disappear accompanied by SC transitions.

The family of $CeTIn_5$ (T = Co, Rh, and Ir), which has a $HoCoGa_5$-type crystal structure (Ref. 16), has attracted a great deal of attention because they possess a relatively high transition temperature (T_c) such as $T_c = 2.3°$ K for $CeCoIn_5$, which is the highest among Ce- and U-based heavy-fermion superconductors. It has been proposed that valence fluctuations are responsible for the superconductivity in some Ce-based compounds. This is due to the fact that in metallic cerium, the phase diagram shows a first-order valence discontinuity line. This line separates the γ-Ce with a $4f$ shell occupation $n_f = 1.0$ from the α-Ce with $n_f \approx 0.9$. The valence transition is isostructural, and the line has a critical end point in the vicinity of $p_{cr} = 2$ GPa and $T_{cr} = 600°$ K. In cases in which p_{cr} is positive, either T_{cr} is very high or T_{cr} is negative, and only a crossover regime is accessible even at $T = 0$. The exceptions are $CeCu_2Si_2$ and $CeCu_2Ge_2$, for which T_{cr} is likely positive although small. In such a situation, the associated low-energy valence fluctuations can mediate superconductivity.

Holmes et al.[10] proposed that the superconducting phase diagram for $CeCu_2(Ge,Si)_2$, shown in Figure 15.14, exhibits a maximum in the transition temperature in close vicinity to a valence-changing critical point. Miyake (Ref. 16) has argued that superconductivity may develop around the region where the critical end point is suppressed to zero, to become a quantum critical point.

The heavy-fermion superconductor $CeCoIn_5$ is a quasi-two-dimensional (2D) system, and the de Haas–van Alphen effect data indicate a quasi-2D Fermi surface. These properties have led to the possibility of a Fulde–Ferrell–Larkin–Ovchinnikov (FFLO) (Refs. 7, 13) superconducting state in $CeCoIn_5$. These states result from the competition between superconducting condensate energy and the magnetic Zeeman energy that lowers the total energy of the electrons in the normal state. This competition is strong when the superconductivity is of a spin-singlet nature. In this case, the superconducting Cooper pairs form with opposite spins, and the electrons cannot lower the total energy of the system by preferentially aligning their spins along the magnetic field. This effect, called Pauli limiting, leads to suppression of superconductivity in the magnetic field. The characteristic

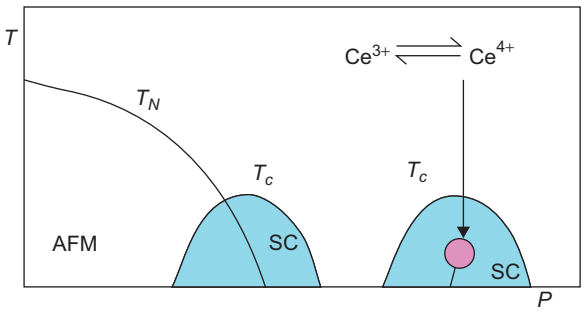

FIGURE 15.14

Schematic phase diagram for $CeCu_2(Ge,Si)_2$ illustrating a possible valence fluctuation critical point beneath the superconducting dome at high pressures.

Reproduced from P. Coleman, (Ref. 5), with the permission of Elsevier.

Pauli field H_P determines the upper limit of the superconducting upper critical field H_{c2}. When Pauli limiting is the dominant mechanism for suppression of superconductivity, a new inhomogeneous superconducting FFLO state would appear at high fields between the normal and the mixed, or the vortex, state below the critical temperature T_{FFLO} with planes of normal electrons that can take advantage of Pauli susceptibility. In the FFLO state, pair breaking due to the Pauli paramagnetic effect is reduced by the formation of a new pairing state $(\mathbf{k}_\uparrow, -\mathbf{k}+\mathbf{q}_\downarrow)$, with $|\mathbf{q}| \sim 2\mu_B H/\hbar v_F$ (v_F is the Fermi velocity) between the Zeeman split parts of the Fermi surface. One of the intriguing features is the T and H phase dependence of the phase boundary between the FFLO and non-FFLO superconducting state. $H^{\mathrm{II}}{}_{\mathrm{FFLO}}$ ($H^{\mathrm{II}}ab$) exhibits an unusually large shift to higher fields at higher temperatures. The results of Bianchi et al.[2] are shown in Figure 15.15.

15.6.2 U-Based Superconducting Compounds

The first two U-based heavy-fermion superconductors, UBe_{13} ($T_c = 0.9°$ K) and UPt_3 ($T_c = 0.54°$ K), were discovered in 1983 by Ott et al. (Ref. 19) and in 1984 by Stewart et al.,[31] respectively. It was evident within a few years that UPt_3 had three superconducting phases, which created great impetus for further study of this unusual heavy-fermion superconductor.

UBe_{13} was the first actinide-based heavy-fermion compound that was found to be a bulk superconductor below approximately 0.9° K. The cubic UBe_{13} is also one of the most fascinating HF superconductors because superconductivity develops out of a highly unusual normal state characterized by a large and strongly T-dependent resistivity. In addition, upon substituting a small amount of Th for U in $U_{1-x}Th_xBe_{13}$, a nonmonotonic evolution of T_c and a second-phase transition of T_{c2} below T_{c1}, the superconducting one, is observed in a critical concentration range of x.

It was also shown that the superconducting state is formed by heavy-mass quasiparticles. This was demonstrated by plotting C_p/T versus T (at low temperatures), which is shown in Figure 15.16. The anomaly at T_c is compatible with the large γ parameter in the normal state at this temperature.

The temperature dependence of the specific heat of UBe_{13} well below T_c was the first indication of the unconventional superconductivity. Figure 15.17 shows the nonexponential but power-law-type

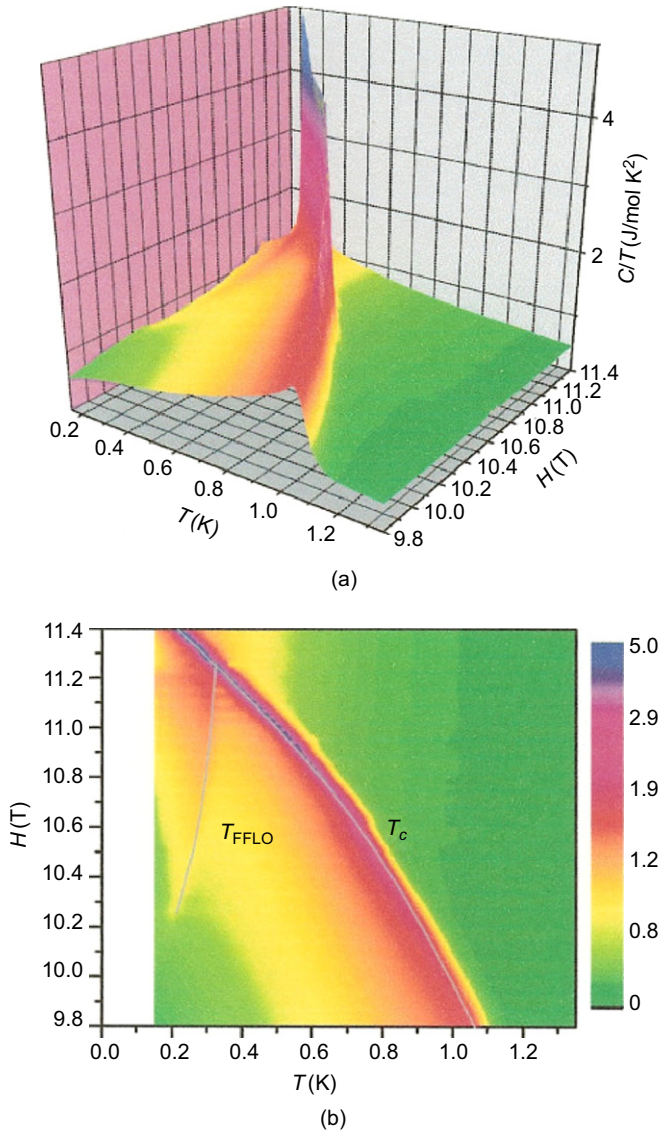

FIGURE 15.15

(a) Electronic specific heat of $CeCoIn_5$ divided by temperature with H^{II} [110] collected with the temperature decay method, as a function of field and temperature. (b) Contour plot of the data in (a) in the *H-T* plane. Gray lines indicate the superconducting phase transition T_c and the FFLO-mixed state T_{FFLO} anomaly. The color scale is the same in (a) and (b).

Reproduced from Bianchi et al.[2] with the permission of the American Physical Society.

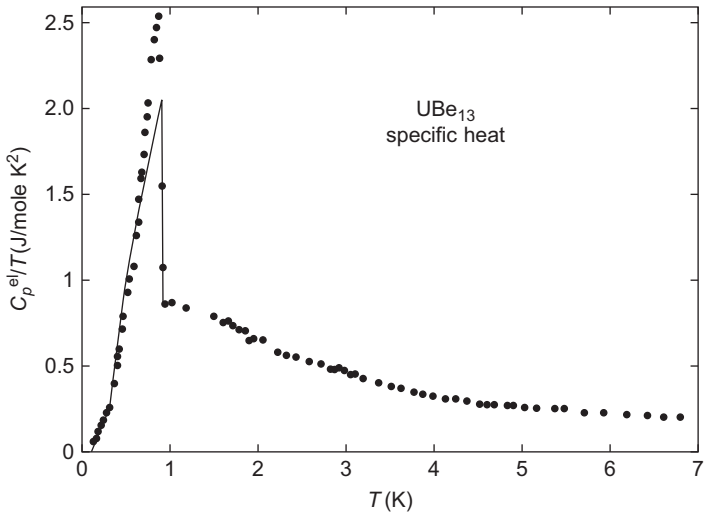

FIGURE 15.16

Electronic specific heat of UBe_{13} below 7° K. The solid line represents the BCS approximation of the anomaly at and below T_c.

Reproduced from Ott[18] with the permission of Elsevier.

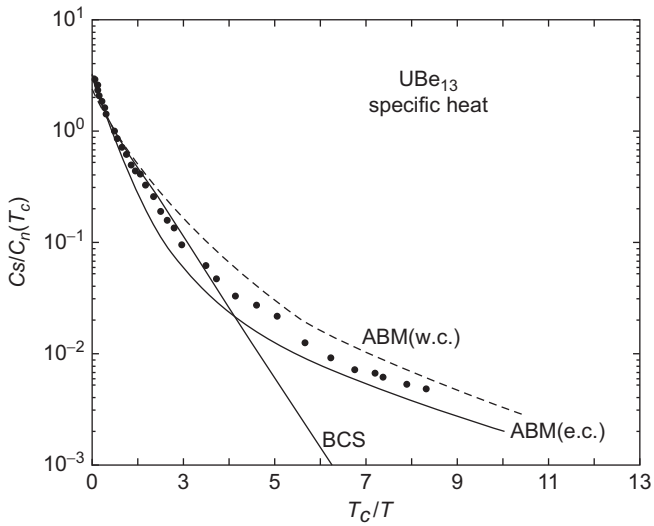

FIGURE 15.17

Normalized electronic specific heat of UBe_{13} below T_c, plotted versus T_c/T. The solid and broken lines represent calculations assuming point nodes in the gap.

Reproduced from Ott[18] with the permission of Elsevier.

decrease of $C_p(T)$ that was interpreted as being the consequence of nodes in the gap of the electronic excitation spectrum.

It was also found that when small amounts of U atoms in UBe_{13} were replaced with other elements, there was a substantial reduction of the critical temperature. T_c is also first substantially reduced with the alloys $U_{1-x}Th_xBe_{13}$ as x is increased. However, when $x > 0.018$, T_c increases again until it passes over a willow maximum at $x = 0.033$ and gradually decreases with a reduced slope when x is further increased. Further, in the range $0.019 < x < 0.05$, a second transition at T_{c2} below T_c was discovered by measuring the specific heat of these alloys at very low temperatures. Measurements of $\rho(T)$ and $\chi(T)$ confirmed that the phase at temperatures below the second anomaly of $C_p(T)$ was superconducting.

The phase diagram of superconductivity of $U_{1-x}Th_xBe_{13}$, from these observations as well as from thermodynamic arguments, is shown in Figure 15.18. One can identify three different superconducting phases: *F*, *L*, and *U*.

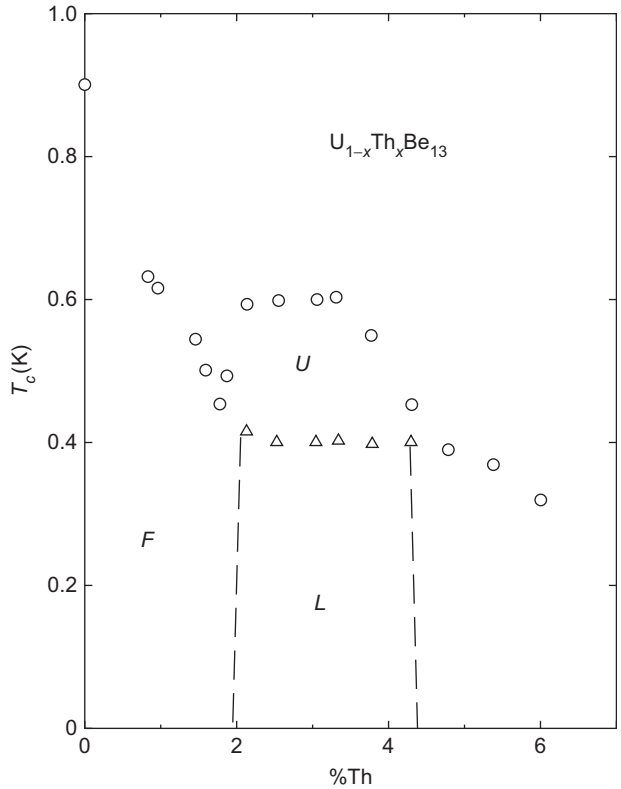

FIGURE 15.18

An *x*, *T* phase diagram for superconducting $U_{1-x}Th_xBe_{13}$ as derived from the measurements of the specific heat. The letters *F*, *L*, and *U* denote three superconducting phases.

Reproduced from Ott[18] with the permission of Elsevier.

Superconductivity has also been discovered in UPt_3, and its alloys, URu_2Si_2; and in UPd_2Al_3 and its alloys, UNi_2Al_3, UGe_2, URhGe, and UIr.

The discovery of superconductivity in UGe_2 in single crystals of UGe_2 under pressure below $P_c \sim 16$ kbar was very surprising. The sensational part of this discovery is that the pressure $P \sim 12$ kbar, where the superconducting temperature $T_S = 0.75°$ K is strongest, the Curie temperature $T_C \sim 35°$ K is two orders of magnitude higher than T_S; superconductivity occurs in a very highly polarized state ($\mu(T \to 0° \text{ K}) \sim \mu_B$).

The superconductivity in UGe_2 disappears above a pressure $P_c \approx 16$ kbar that coincides with the pressure at which the ferromagnetism is suppressed. The pressure-temperature phase diagram of UGe_2 is shown in Figure 15.19.

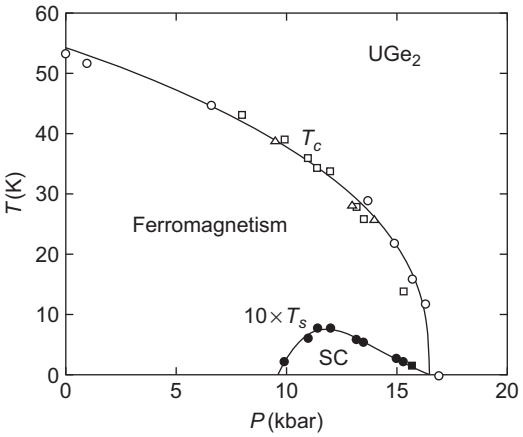

FIGURE 15.19

The pressure-temperature phase diagram of UGe_2.

Reproduced from Demuer et al.[4] with permission of Elsevier.

15.7 OTHER HEAVY-FERMION SUPERCONDUCTORS

15.7.1 $PrOs_4Sb_{12}$

The filled skutterdite $PrOs_4Sb_{12}$ becomes superconducting at $T_c = 1.85°$K. It appears to involve heavy-fermion quasiparticles with effective mass $m^* \sim 50\, m_e$. There is speculation that the quadrupolar fluctuations play a role in the heavy-fermion superconductivity of $PrOs_4Sb_{12}$. The ground state of Pr^{3+} ions in the cubic CEF appears to be the Γ_3 nonmagnetic doublet. Therefore, the heavy-fermion behavior possibly involves the interaction of the Pr^{3+} Γ_3 quadrupole moments and the charges of the conduction electrons. In such a case, the quadrupolar fluctuations would play a role in the heavy-fermion superconductivity of $PrOs_4Sb_{12}$.

The variation of C at low temperature and the magnetic phase diagram inferred from C, the resistivity and magnetization, show that there was a doublet ground state. The two distinct superconducting anomalies in C provide evidence of two superconducting critical temperatures at $T_{C1} = 1.75°$ K and $T_{C2} = 1.85°$ K. This could arise from a weak lifting from of the ground-state degeneracy, which supports the theory of quadrupolar pairing; i.e., superconductivity in $PrOs_4Sb_{12}$ is neither of electron–phonon nor of magnetically mediated origin.

The H-T superconducting phase diagram of $PrOs_4Sb_{12}$ determined by specific heat measurements is shown in Figure 15.20.

15.7.2 $PuCoGa_5$

The discovery of superconductivity in the transuranium compound $PuCoGa_5$ with $T_c \approx 18.5°$ K, which is by far the highest critical temperature for any heavy-fermion superconductor, has attracted considerable attention. $PuCoGa_5$ crystallizes in the $HoCoGa_5$ structure, the same type as the $CeMIn_5$ materials. The *H-T* phase diagram of $PuCoGa_5$, inferred from the heat capacity data as a function of temperature in a magnetic field applied along the three orthogonal directions, is shown in Figure 15.21.

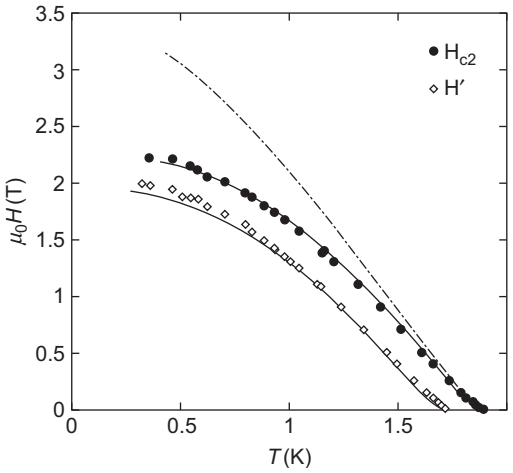

FIGURE 15.20

H-T superconducting phase diagram of $PrOs_4Sb_{12}$. The field dependences of T_{c1} and T_{c2} are identical. The dashed-dotted line is the same fit with the same parameters as the other lines but without paramagnetic limitation.

Reproduced from Measson et al.[15] with the permission of Elsevier.

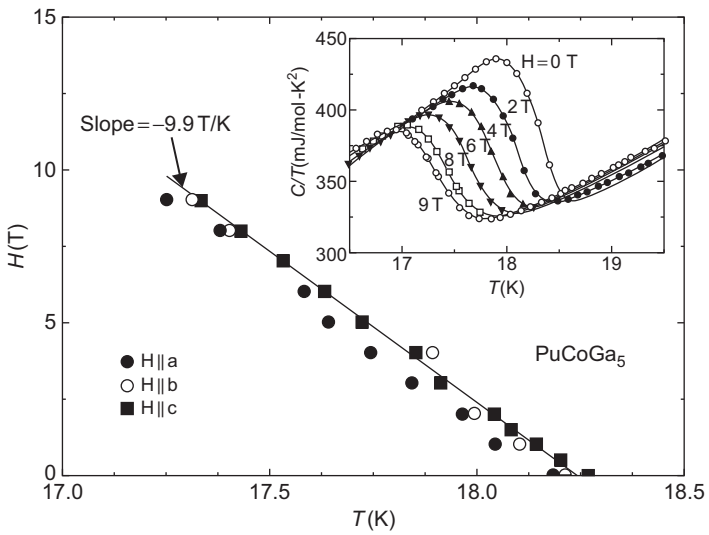

FIGURE 15.21

H-T diagram of $PuCoGa_5$ inferred from single-crystal heat capacity measurements with magnetic field applied along three orthogonal directions. The inset shows representative heat capacity data from which $T_c(H)$ was inferred.

Reproduced from J.L. Sarrao et al. (Ref. 23), with the permission of Elsevier.

15.7.3 $PuRhGa_5$

The discovery of superconductivity in $PuRhGa_5$ with $T_c \approx 9°$ K was reported by Wastin et al. (Ref. 34). $PuRhGa_5$ crystallizes in the tetragonal $HoCoGa_5$ structure with the lattice parameters $a =$ 4.2354 Å and $c = 6.7939$ Å. This structure has a two-dimensional feature, where alternating $PuGa_3$ and $RhGa_2$ layers are stacked along the c-axis. There are two crystallographically inequivalent Ga sites in this structure, which are denoted Ga(1) (the 1c site) and Ga(2) (the 4i site), respectively. The Ga(1) site is surrounded by four Pu atoms in the c plane, whereas the Ga(2) site is surrounded by two Pu and two Rh atoms in the a plane.

The high-pressure measurements on $PuRhGa_5$ are shown in Figure 15.22, in which the electrical resistance is plotted against temperature for pressures up to 18.7 GPa. This figure displays a metallic shape in the normal state, but an NFL behavior ($\rho(T) \sim T^{1.3}$) develops up to 50–60° K. The inset of Figure 15.22 shows the plot of T_c of both $PuRhGa_5$ and $PuCoGa_5$ against pressure.

The variation of T_c as a function of pressure (Figure 15.22) suggests that the pairing mechanism is differently affected by pressure for the two materials. The layered crystal structure associated with the quasi-2D Fermi surface calculated for these materials suggests that anisotropic properties might be the cause for this difference.

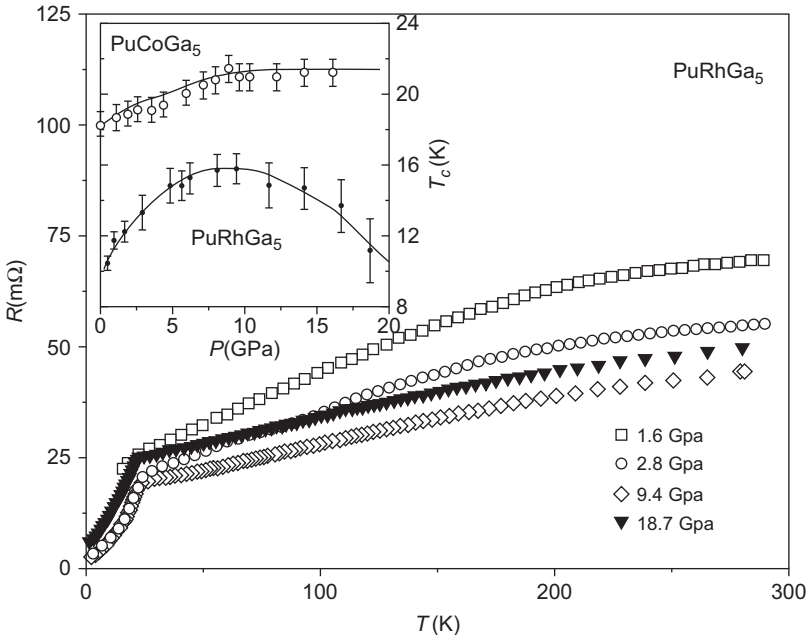

FIGURE 15.22

Evolution of the electrical resistance of $PuRhGa_5$ crystal up to 18.7 GPa. The inset shows T_c behavior of $PuCoGa_5$ as a function of the applied pressure.

Reproduced from Griveau et al.[8] with the permission of Elsevier.

The (T-P) phase diagram of $PuRhGa_5$ and $PuCoGa_5$ can be compared to that of $CeCoIn_5$. In these isostructural compounds, the superconducting transition temperature increases with increasing pressure and reaches a maximum before decreasing at higher pressure. The NFL behavior is also maintained over a large range of pressure.

15.7.4 Comparison between Cu and Pu Containing High-T_c Superconductors

Recently, Wachter[33] compared the Cu "high T_c superconductors" with equivalent measurements on "high T_c" $PuCoGa_5$ and $PuRhGa_5$. He observed the following common features. First, in all materials, spin pseudogaps were observed, which necessitates at least antiferromagnetic short-range order, i.e., in clusters. Second, all Cu and Pu superconductors are of mixed valence, as photoemission data have shown. The majority ions (Cu or Pu) are magnetic, and the minority ions are nonmagnetic and act as spin holes. Only short-range correlations remain because these spin holes have a concentration of 10% and hence dilute the antiferromagnetic order. According to Wachter, two dimensionality is not essential and n- or p-type conductivity is not important.

15.8 THEORIES OF HEAVY-FERMION SUPERCONDUCTIVITY

The superfluid ^{3}He, the physical properties of which were extensively studied prior to the discovery of heavy-fermion superconductivity, exhibited gap anisotropy and nodal structures like some heavy-fermion compounds. After the discovery of heavy-fermion superconductors, it was natural to compare them with superfluid ^{3}He to be able to understand the former. However, there are many differences between the two systems. For example, the presence of a crystal field and the fact that charged particles are paired in heavy fermions instead of pairing of the neutral atoms in ^{3}He are important. In addition, the strong correlation effects and the spin-orbit interaction in heavy-fermion systems are major factors to be considered.

In heavy-fermion compounds, the f-shell electrons are strongly correlated. These f electrons determine the properties of the quasiparticles at the Fermi level, which gives rise to a large effective mass. It is generally believed that superconductivity is mainly by the heavy quasiparticles. These quasiparticles with f characters would have difficulty forming ordinary s-wave Cooper pairs, characteristic of the BCS theory of superconductivity, due to the strong Coulomb repulsion. To avoid a large overlap of the wave functions of the paired particles, the system would rather choose an anisotropic channel, such as a p-wave spin triplet (as is done in superfluid ^{3}He) or a d-wave spin singlet state to form pairs.

We cannot review here in detail the theory of superconductivity of each heavy-fermion compound. In addition, heavy-fermion systems are one of the areas in physics where the experimentalists are well ahead of the theorists and superconductivity in various heavy-fermion compounds has a different origin.

15.9 KONDO INSULATORS

15.9.1 Brief Review

The strongly correlated f-electron materials called Kondo insulators have recently attracted much attention because of their unusual physical properties. At high temperatures, they behave like metals with a local magnetic moment, whereas at low temperatures, they behave as paramagnetic insulators

with a small energy gap at the Fermi level. It appears that a gap in the conduction band opens at the Fermi energy as the temperature is reduced. Despite intensive theoretical and experimental studies, the mechanism of gap formation is still unclear, and there is considerable controversy on how to describe the physics of Kondo insulators. We will concentrate on the $4f$ and $5f$ compounds, i.e., those f-element compounds that are in a certain sense "valence" compounds. The general properties of these materials are characterized by a small gap. The f elements that are present in these compounds have unstable valence, with the valence corresponding to the nonmagnetic f state of the element satisfying the valence requirements of the other elements in the material. The Kondo insulator can be viewed as a limiting case of the correlated electron lattice: exactly one half-filled band interacting with one occupied f-level. This can also be viewed as the limiting case of the Kondo lattice with one conduction electron to screen one moment at each site. However, there has been no clear definition of Kondo insulators, and this situation stems from the confusion over how to understand various types of Kondo insulators consistently.

Following is a variety of Kondo insulators, some of which are semiconductors that become Kondo insulators with application of pressure: CeNiSn, $Ce_3Bi_4Pt_3$, CeRhAs, CeRhSb, CeNiSn, $CeRu_4Sn_6$, URu_2Sn, $CeFe_4P_{12}$, $CeRu_4P_{12}$, $CeOs_4Sb_{12}$, UFe_4P_{12}, TmSe, URu_2Sn, YbB_{12}, SmB_6, and SmS.

A detailed review of the experimental properties of each one of these Kondo insulators is available in Misra.[16]

15.9.2 Theory of Kondo Insulators

The Anderson Lattice Model

The Anderson lattice model provides a basic description of the electronic properties of the heavy-fermion materials. The solution of the model at half-filling is expected to exhibit an indirect gap in the density of states. The chemical potential lies directly in the gap making the system semiconducting. Thus, if there are four states per atom—two states per atom in the upper hybridized band and two states per atom in the lower hybridized band—then at half-filling, two electrons per atom completely fill the doubly degenerate lower hybridized band and the noninteracting system is semiconducting. According to Luttinger's theorem, if the interactions are turned on adiabatically so that perturbation theory converges, the ground state of the interacting system will remain insulating. The Hamiltonian can be written as

$$H = H_f + H_d + H_{fd}, \tag{15.56}$$

where H_f is the Hamiltonian of the lattice of localized f electrons, H_d is the Hamiltonian of the conduction electron states, and H_{fd} is the hybridization Hamiltonian,

$$H_f = \sum_{i,\alpha} E_f f^\dagger_{i,\alpha} f_{i,\alpha} + \sum_{i,\alpha,\beta} \frac{U_{ff}}{2} f^\dagger_{i,\alpha} f^\dagger_{i,\beta} f_{i,\beta} f_{i,\alpha}, \tag{15.57}$$

$$H_d = \sum_{\mathbf{k},\alpha} \varepsilon_d(\mathbf{k}) d^\dagger_{\mathbf{k},\alpha} d_{\mathbf{k},\alpha}, \tag{15.58}$$

and

$$H_{fd} = N_s^{-1/2} \sum_{i,\mathbf{k},\alpha} [V(\mathbf{k}) \exp(-i\mathbf{k}\cdot\mathbf{R}_i) f^\dagger_{i,\alpha} d_{\mathbf{k},\alpha} + V^*(\mathbf{k}) \exp(i\mathbf{k}\cdot\mathbf{R}_i) d^\dagger_{\mathbf{k},\alpha} f_{i,\alpha}]. \tag{15.59}$$

Here, E_f is the binding energy of a single f electron to a lattice site, and U_{ff} is the Coulomb repulsion between a pair of f electrons located on the same lattice site. Due to the spin and orbital degrees of freedom, the total degeneracy of each f orbital is 14. This degeneracy can be lifted by spin-orbit coupling and crystal field splitting. We will consider the degeneracy of the lowest f multiplet to be $N = 2$. The operators $f^\dagger_{i\alpha}(f_{i\alpha})$ create (destroy) an f electron at site i with a combined spin-orbit label α. The summation is over all lattice sites and all degeneracy labels. $\varepsilon_d(\mathbf{k})$ is the dispersion relation for the d-bands; the operators $d^\dagger_{\mathbf{k}\alpha}(d_{\mathbf{k}\alpha})$ create and annihilate an electron in the αth d sub-band state labeled by the Bloch wave vector $\mathbf{k}$. The hybridization between the f states and the states of the d-band is governed by H_{fd}. The first term represents a process in which a conduction electron in the Bloch state $\mathbf{k}$ hops into the f orbital located at site i. However, α is conserved in the process. The Hermitian conjugate term describes an electron in the f orbital at site i tunneling into the conduction band state labeled by the Bloch state $\mathbf{k}$. The summation runs over the total number of lattice sites N_s and over the $\mathbf{k}$ values of the first Brillouin zone.

Riseborough's Theory

Riseborough (Ref. 20) showed that the noninteracting Hamiltonian ($U_{ff} \to 0$) is exactly soluble and the electronic states fall into two quasiparticle bands of mixed f and conduction band character. He showed that in this limit, the binding energy of the f-levels falls within the width of the unhybridized conduction band, which has a width of $2\ W = 12t$ in the tight-binding approximation. The indirect gap is between the zone boundary of the upper branch and the $k = 0$ state of the upper branch. The direct gap occurs for k values halfway along the body diagonal and has a magnitude of $2V$. A sketch of the hybridized bands is shown in Figure 15.23. Each band can contain a maximum of $2N$ electrons.

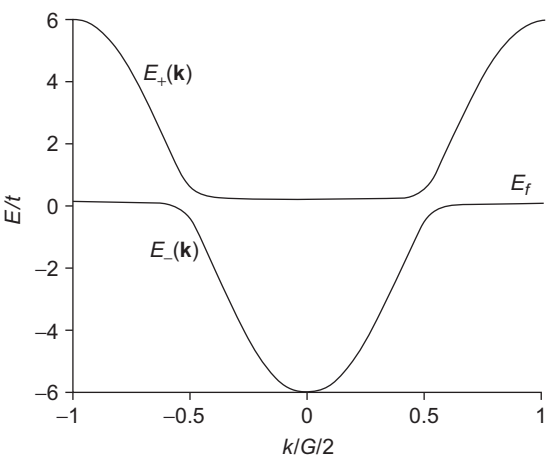

FIGURE 15.23

Sketch of the hybridized band structure, for k vectors along the body diagonal of the first Brillouin zone.

Reproduced from Riseborough[20] with the permission of Taylor & Francis Ltd.

Thus, the noninteracting system is a semiconductor. If the interactions are turned on adiabatically, Luttinger's theorem implies that the ground state of the system will be an insulator. In the mean-field approximation, one can use the slave boson technique described earlier. This approach to the $U_{ff} \to \infty$ limit of the Anderson lattice model projects the states of double f occupancy. The f electron operators are replaced by a product of an f quasiparticle operator and a slave boson field,

$$\begin{aligned} f^\dagger_{i,\alpha} &= \tilde{f}^\dagger_{i,\alpha} b_i, \\ f_{i,\alpha} &= b^\dagger_i \tilde{f}^\dagger_{i,\alpha}, \end{aligned} \tag{15.60}$$

where b_i and $b^\dagger_i$ are the annihilation and creation operators for the site i, and the f quasiparticle operators are $\tilde{f}^\dagger_{i,\alpha}$ and $\tilde{f}_{i,\alpha}$. These operators satisfy the constraints

$$\sum_\alpha \tilde{f}^\dagger_{i,\alpha} \tilde{f}_{i,\alpha} + b^\dagger_i b_i = Q_i = 1. \tag{15.61}$$

The slave boson field satisfies the equation of motion

$$i\hbar\frac{\partial}{\partial t}(b_i^\dagger) = \lambda_i b_i^\dagger + \frac{1}{N_s^{1/2}}\sum_{\mathbf{k},\alpha} V(\mathbf{k})\exp[i\mathbf{k}\cdot\mathbf{R}_i]\widetilde{f}_{i,\alpha}^\dagger d_{\mathbf{k},\alpha}. \tag{15.62}$$

The lowest-order approximation, the terms of zeroth order in the boson fluctuation operators b_i, is retained. If b_0 is finite, this corresponds to a time-independent macroscopic equation of the $k = 0$ state that is equivalent to assuming that the boson field has undergone Bose–Einstein condensation. In this approximation, Eq. (15.62) can be written as (Problem 15.6)

$$\lambda_i b_0^* = \frac{-1}{N_s^{1/2}}\sum_{\mathbf{k},\alpha} V(\mathbf{k})\exp[i\mathbf{k}\cdot\mathbf{R}_i]\langle\widetilde{f}_{i,\alpha}^\dagger d_{\mathbf{k},\alpha}\rangle. \tag{15.63}$$

Here, b_0 and λ_i can be determined self-consistently from Eqs. (15.62) and (15.63). The hybridization matrix element is renormalized through

$$\widetilde{V}(\mathbf{k}) = b_0 V(\mathbf{k}), \tag{15.64}$$

and the f-level energy is renormalized through

$$\widetilde{E}_f = E_f + \lambda. \tag{15.65}$$

This moves the quasiparticle component of the f structure from the incoherent bare f-level component of the density of states to a position near the chemical potential. It can be shown that the quasiparticle dispersion relations are obtained as (Problem 15.7)

$$E_\pm(\mathbf{k}) = \frac{1}{2}[\widetilde{E}_f + \varepsilon_d(\mathbf{k}) \pm ([\widetilde{E}_f - \varepsilon_d(\mathbf{k})]^2 + 4|\widetilde{V}(\mathbf{k})|^2)^{1/2}]. \tag{15.66}$$

In this formulation, the amplitude of the slave boson condensate b_i is temperature dependent and vanishes at a critical temperature, T_c, for the semiconductor system. It can be shown that

$$k_B T_c = 1.14W\exp\left[\frac{E_f - \mu}{N\Delta}\right], \tag{15.67}$$

where $\Delta = |V|^2/W$, W represents approximately half the width of the conduction band, and the direct gap has a magnitude of $2V$. It is interesting to note that this temperature dependence is related to the Kondo temperature, in which the effects of both band edges are taken into account.

It may be noted that the slave boson mean-field theory is exact only when the degeneracy of the f-level approaches infinity. In addition, it is valid only when the lower band is fully occupied, which is true only for some Kondo insulators but not others, such as SmB_6. The effect of the magnetic field gives rise to a Zeeman splitting of the quasiparticle bands, reducing the hybridization gap. It has been shown by using the periodic Anderson lattice (in the limit of infinite spatial dimensions, $d \to \infty$) that the semiconductor-to-metal transition associated with the high field closing the gap may be of the first order.

PROBLEMS

15.1. The Schrieffer-Wolff transformation[24] can be easily used to relate the Anderson model of a localized magnetic moment to that of Kondo. The two models can be shown to be equivalent in small $s-f$ mixing. The Anderson Hamiltonian for a single localized orbital f is

$$\hat{H} = \sum_{k\sigma}\in_k n_{k\sigma} + \sum_\sigma \in_f n_{f\sigma} + Un_{f\uparrow}n_{f\downarrow} + \sum_{k\sigma}[V_{kf}\hat{C}_{k\sigma}^\dagger\hat{C}_{f\sigma} + V_{kf}^*\hat{C}_{f\sigma}^\dagger\hat{C}_{k\sigma}] = \hat{H}_0 + \hat{H}_1, \tag{1}$$

where $\in_k$ and $\in_f$ are the one-electron energies of the conduction and localized orbitals, measured relative to the Fermi energy, and $\hat{H}_0$ is the sum of the first three terms in Eq. (1). The model can be characterized by two dimensionless ratios

$$r_\pm \equiv \Gamma_\pm / |\in_\pm|, \tag{2}$$

where

$$\begin{aligned} \in_f &= \in_f + U, \quad \alpha = +, \\ &= \in_f, \qquad \alpha = -, \end{aligned} \tag{3}$$

and

$$\Gamma_\alpha = \pi N(\in_\alpha) |V_{kf}|^2_{AVE}. \tag{4}$$

$N(\in_\alpha)$ is the density of band states in the perfect crystal at energy $\in_\alpha$, and the matrix elements are averaged over k states of this energy. If $\in_+ > 0$ and $\in_- < 0$, then for $V_{kf} \to 0$, the ground state is given by the filled Fermi sea and a single electron occupying the f orbital. A localized moment occurs even at zero temperature because the states with f-electron spin $\uparrow$ and $\downarrow$ are degenerate. For $r_\alpha \ll 1$, these two spin states are mixed by electrons hopping on and off the f orbital due to V. Because arbitrarily small energy denominators $\in_k - \in_{k'} \simeq 0$ occur in fourth and higher orders of V, V cannot be treated directly by perturbation theory. However, the interactions that dominate the dynamics of the system for $r_\alpha \ll 1$ can be isolated. Show that one can perform a canonical transformation,

$$\overline{H} \equiv e^S H e^{-S}, \tag{5}$$

by requiring that V_{kf} is eliminated to the first order, where

$$[H_0, S] = H_1. \tag{6}$$

Show from Eqs. (4) and (6) that

$$S = \sum_{k\sigma\alpha} \frac{V_{kf}}{\in_k - \in_\alpha} n^\alpha_{f,-\sigma} C^\dagger_{k\sigma} C_{f\sigma} - H.C., \tag{7}$$

where the projection operators $n^\alpha_{f,-\sigma}$ are defined by

$$\begin{aligned} n^\alpha_{f,-\sigma} &= n_{f,-\sigma}, \qquad \alpha = +, \\ &= 1 - n_{f,-\sigma}, \quad \alpha = -. \end{aligned} \tag{8}$$

Show also that in the limit $r_\alpha \ll 1$,

$$\overline{H} \approx H_0 + H_2, \tag{9}$$

where

$$H_2 = \frac{1}{2}[S, H_1] \approx H_{ex} = -\sum_{kk'} J_{k'k} (\Psi^\dagger_{k'} \mathbf{S} \Psi_k) \cdot (\Psi^\dagger_f \mathbf{S} \Psi_f), \tag{10}$$

where $2\mathbf{S} = \tau$ are the Pauli spin matrices, Ψ_k and Ψ_f are the field operators

$$\Psi_k = \begin{pmatrix} c_{k\uparrow} \\ c_{k\downarrow} \end{pmatrix}, \Psi_d = \begin{pmatrix} c_{f\uparrow} \\ c_{f\downarrow} \end{pmatrix}, \tag{11}$$

and

$$J_{k'k} = V_{k'f}V_{fk}\{(\in_k - \in_+)^{-1} + (\in_{k'} - \in_+)^{-1} - (\in_{k'} - \in_-)^{-1} - (\in_{k'} - \in_-)^{-1}\}. \tag{12}$$

For k and $k' \simeq k_F$, $J_{kk'}$ is given by

$$J_{k_Fk_F} \equiv J_0 = 2|V_{k_Ff}|^2 \frac{U}{\in_f(\in_f + U)}. \tag{13}$$

This coupling is antiferromagnetic. If there is an f electron at every site of the lattice, from Eq. (10), the f-electron degrees of freedom are represented by localized spins.

15.2. Show that

$$g_0(i\omega_n)^{-1} = i\omega_n + \mu + G(i\omega_n)^{-1} - R[G(i\omega_n)^{-1}]. \tag{1}$$

Here, $G(i\omega_n)$, the on-site interacting Green's function, is calculated from the effective action S_{eff} defined in Eq. (15.14),

$$G(\tau - \tau') = -<TC(\tau)C^{\dagger}(\tau')>_{S_{eff}} \tag{2}$$

$$G(i\omega_n) = \int_0^{\beta} d\tau G(\tau)e^{i\omega_n\tau}, \omega_n \equiv \frac{(2n+1)\pi}{\beta}. \tag{3}$$

Here, $R(G)$ is the reciprocal function of the Hilbert transform of the density of states corresponding to the lattice. The noninteracting density of states is

$$D(\in) = \sum_{\mathbf{k}} \delta(\in - \in_{\mathbf{k}}), \tag{4}$$

where

$$\in_{\mathbf{k}} \equiv \sum_{ij} t_{ij}e^{i\mathbf{k}\cdot(\mathbf{R}_i - \mathbf{R}_j)}. \tag{5}$$

The Hilbert transform $\overline{D}(\xi)$ and its reciprocal function R are defined by

$$\overline{D}(\xi) = \int_{-\infty}^{\infty} d\in \frac{D(\in)}{\xi - \in} \tag{6}$$

and

$$R\,[\overline{D}(\xi)] = \xi. \tag{7}$$

In principle, G can be computed as a functional of g_0, using the impurity action S_{eff}. Thus, Eqs. (15.14), (1), and (2) form a complete system of functional equations for the on-site Green's function G and the Weiss function g_0.

15.3. The Hamiltonian of a three-dimensional Kondo–Heisenberg model on a cubic lattice is

$$H = \sum_k \in_{\mathbf{k}} C^{\dagger}_{\mathbf{k}\alpha}C_{\mathbf{k}\alpha} + \frac{J_K}{2}\sum_r \overrightarrow{S}_r \cdot C^{\dagger}_{r\alpha}\overrightarrow{\sigma}_{\alpha\alpha'}C_{r\alpha'} + J_H \sum_{<rr'>} \overrightarrow{S}_r \cdot \overrightarrow{S}_{r'}. \tag{1}$$

Here, $C_{\mathbf{k}\alpha}$ is the conduction electron destruction operator, $\overrightarrow{S}_r$ are the spin-1/2 local moments, and summation over repeated spin indices α is implied. In a fermionic "slave-particle" representation of the local moments

$$\overrightarrow{S}_r = 1/2 f^\dagger_{r\alpha} \overrightarrow{\sigma}_{\alpha\alpha'} f_{r\alpha'}, \tag{2}$$

and $f_{r\alpha}$ is a spinful fermion destruction operator at site r. The decoupling of the Kondo and the Heisenberg exchange is made using two auxiliary fields by a saddle-point approximation, and the mean-field Hamiltonian is

$$H_{mf} = \sum_{\mathbf{k}} \in_{\mathbf{k}} C^\dagger_{\mathbf{k}\alpha} C_{\mathbf{k}\alpha} - \chi_0 \sum_{<rr'>} (f^\dagger_{r\alpha} f_{r'\alpha} + H.c.) + \mu_f \sum_r f^\dagger_{r\alpha} f_{r\alpha} - b_0 \sum_{\mathbf{k}} (C^\dagger_{\mathbf{k}\alpha} f_{\mathbf{k}\alpha} + H.C.). \tag{3}$$

Here, b_0 and χ_0 are assumed to be real and additional constants to H are dropped. Show that the mean-field parameters b_0, χ_0, and μ_f are obtained from

$$1 = <f^\dagger_{r\alpha} f_{r\alpha}>, \tag{4}$$

$$b_0 = J_K/2 <C^\dagger_{r\alpha} f_{r\alpha}>, \tag{5}$$

$$\chi_0 = J_H/2 <f^\dagger_{r\alpha} f_{r'\alpha}>, \tag{6}$$

where r and r' are nearest neighbors. At zero temperature, in the Fermi-liquid (FL) phase, χ_0, b_0, and μ_0 are nonzero. In the FL^* phase, $b_0 = \mu_0 = 0$, but $\chi_0 \neq 0$. In this state, the conduction electrons are decoupled from the local moments and form a small Fermi surface. The local-moment system is described as a spin fluid with a Fermi surface of neutral spinons.

15.4. In Problem 15.3, the mean-field is diagonalized by the transformation (Senthil et al.[26]),

$$C_{\mathbf{k}\alpha} = u_{\mathbf{k}} \gamma_{\mathbf{k}\alpha+} + v_{\mathbf{k}} \gamma_{\mathbf{k}\alpha-} \tag{1}$$

and

$$f_{\mathbf{k}\alpha} = v_{\mathbf{k}} \gamma_{\mathbf{k}\alpha+} - u_{\mathbf{k}} \gamma_{\mathbf{k}\alpha-}. \tag{2}$$

Show that the Hamiltonian (Eq. 3 in Problem 15.3) can be written in terms of the new fermionic operators $\gamma_{\mathbf{k}\alpha\pm}$,

$$H_{mf} = \sum_{\mathbf{k}\alpha} E_{\mathbf{k}+} \gamma^\dagger_{\mathbf{k}\alpha+} \gamma_{\mathbf{k}\alpha+} + E_{\mathbf{k}-} \gamma^\dagger_{\mathbf{k}\alpha-} \gamma_{\mathbf{k}\alpha-}, \tag{3}$$

where

$$E_{\mathbf{k}\pm} = \frac{\in_{\mathbf{k}} + \in_{\mathbf{k}f}}{2} \pm \sqrt{\left(\frac{\in_{\mathbf{k}} - \in_{\mathbf{k}f}}{2}\right)^2 + b_0^2}. \tag{4}$$

Here, $\in_{\mathbf{k}f} = \mu_f - \chi_0 \sum_{a=1,2,3} \cos(k_a)$. The $u_{\mathbf{k}}, v_{\mathbf{k}}$ are determined by

$$u_{\mathbf{k}} = -\frac{b_0 v_{\mathbf{k}}}{E_{\mathbf{k}+} - \in_{\mathbf{k}}}, \quad u^2_{\mathbf{k}} + v^2_{\mathbf{k}} = 1. \tag{5}$$

15.5. The metals of the rare-earth (lanthanide) group have very small $4f^n$ magnetic cores immersed in a sea of conduction electrons from the $6s$–$6p$ bands. The magnetic properties of these metals can be understood in detail in terms of an indirect exchange interaction between the magnetic

cores via the conduction electrons. If the spins of the local magnetic moments at $\mathbf{r} = \mathbf{r}_i$ are $\mathbf{S}_i$ and at $\mathbf{r} = \mathbf{r}_j$ are $\mathbf{S}_j$, the second-order interaction between the two spins is given by

$$H''(\mathbf{x}) = \sum_{\mathbf{k}\mathbf{k}'ss'}{}' \frac{<\mathbf{k}s\,|H|\,\mathbf{k}'s'><\mathbf{k}'s'\,|H|\,\mathbf{k}s>}{\varepsilon_{\mathbf{k}} - \varepsilon_{\mathbf{k}'}}. \tag{1}$$

Here,

$$H = \sum_{\mathbf{k}\mathbf{k}'ss'} \left[\int d^3x \phi^*_{\mathbf{k}'s'}(\mathbf{x}) A(\mathbf{x}-\mathbf{r}_i)\mathbf{S}\cdot\mathbf{S}_i\phi_{\mathbf{k}s}(\mathbf{x})\right] c^\dagger_{\mathbf{k}'s'}c_{\mathbf{k}s}, \tag{2}$$

where $A(\mathbf{x}-\mathbf{r}_i)$ is the interaction (which is proportional to the delta function) between the spin of the electron $\mathbf{S}$ and the spin $\mathbf{S}_i$ of the local moment at site $\mathbf{r}_i$. Here, $\phi_{\mathbf{k}s}$ are the Bloch functions $\phi_{\mathbf{k}s} = \phi_{\mathbf{k}}|s>$, and $\mathbf{S}$ operates on the spin part of $\phi_{\mathbf{k}s}$. Show that Eq. (2) can be rewritten as

$$H = \frac{1}{2}\sum_{\mathbf{k},\mathbf{k}'} e^{i(\mathbf{k}-\mathbf{k}')\cdot\mathbf{R}_i} J(\mathbf{k}',\mathbf{k})[S^\dagger_i c^\dagger_{\mathbf{k}'\downarrow}c_{\mathbf{k}\uparrow} + S^-_i c^\dagger_{\mathbf{k}'\uparrow}c_{\mathbf{k}\downarrow} + S^z_i(c^\dagger_{\mathbf{k}'\uparrow}c_{\mathbf{k}\uparrow} - c^\dagger_{\mathbf{k}'\downarrow}c_{\mathbf{k}\downarrow}], \tag{3}$$

where

$$J(\mathbf{k},\mathbf{k}') = \int d^3x\, \phi^*_{\mathbf{k}'}(\mathbf{x})A(\mathbf{x})\phi_{\mathbf{k}}(\mathbf{x}). \tag{4}$$

If

$$A(\mathbf{x}) = J\delta(\mathbf{x}), \tag{5}$$

$$J(\mathbf{k}',\mathbf{k}) = J. \tag{6}$$

From Eqs. (1), (2), and (6), show that

$$H''(\mathbf{x}) = \sum_{\mathbf{s}}(\mathbf{S}\cdot\mathbf{S}_i)(\mathbf{S}\cdot\mathbf{S}_j)mJ^2\hbar^{-2}(2\pi)^{-6}P\int_o^{k_F} d^3k \int_{k_F}^{\infty} d^3k' \frac{e^{-i(\mathbf{k}-\mathbf{k}').\mathbf{x}}}{k^2 - k'^2} + cc. \tag{7}$$

The sum over electron spin states is done with the help of the standard relation between Pauli operators,

$$(\sigma\cdot\mathbf{S}_i)(\sigma\cdot\mathbf{S}_j) = \mathbf{S}_i\cdot\mathbf{S}_j + i\sigma\cdot\mathbf{S}_i\times\mathbf{S}_j. \tag{8}$$

Because the trace of any component of σ vanishes,

$$\sum_{\mathbf{s}}(\mathbf{S}\cdot\mathbf{S}_i)(\mathbf{S}\cdot\mathbf{S}_j) = \frac{1}{2}\mathbf{S}_i\cdot\mathbf{S}_j. \tag{9}$$

From Eqs. (7) and (9), by performing the integrations, show that

$$H''(\mathbf{x}) = \frac{4J^2mk_F^4}{(2\pi)^3\hbar^2 r_{ij}^4}[2k_Fr_{ij}\cos(2k_Fr_{ij}) - \sin(2k_Fr_{ij})]\mathbf{S}_i\cdot\mathbf{S}_j. \tag{10}$$

The density of conduction electrons,

$$n_c = \frac{k_F^3}{3\pi^2}. \tag{11}$$

From Eqs. (10) and (11), we obtain the RKKY interaction,

$$H_{\mathrm{RKKY}} = -\frac{9\pi}{8} n_c^2 \frac{J^2}{\varepsilon_F} \sum_{<ij>} \frac{\mathbf{S}_i \cdot \mathbf{S}_j}{r_{ij}^3} \left[2k_F \cos(2k_F r_{ij}) - \frac{\sin(2k_F r_{ij})}{r_{ij}} \right], \tag{12}$$

where a factor of ½ has been multiplied to avoid double counting of i and j. The spin–spin interaction is long ranged and changes its sign depending on the distance between the pair of spins.

15.6. The slave boson field satisfies the equation of motion

$$i\hbar \frac{\partial}{\partial t}(b_i^\dagger) = \lambda_i b_i^\dagger + \frac{1}{N_s^{1/2}} \sum_{\mathbf{k},\alpha} V(\mathbf{k}) \exp[i\mathbf{k} \cdot \mathbf{R}_i] \tilde{f}_{i,\alpha}^\dagger d_{\mathbf{k},\alpha}. \tag{1}$$

The lowest-order approximation, the terms of zeroth order in the boson fluctuation operators b_i, is retained. If b_0 is finite, this corresponds to a time-independent macroscopic equation of the $k = 0$ state, which is equivalent to assuming that the boson field has undergone Bose–Einstein condensation. In this approximation, show that Eq. (1) can be rewritten as

$$\lambda_i b_0^* = \frac{-1}{N_s^{1/2}} \sum_{\mathbf{k},\alpha} V(\mathbf{k}) \exp[i\mathbf{k} \cdot \mathbf{R}_i] \langle \tilde{f}_{i,\alpha}^\dagger d_{\mathbf{k},\alpha} \rangle. \tag{2}$$

15.7. Show that in the slave boson mean-field theory, the quasiparticle dispersion relations are obtained as

$$E_\pm(\mathbf{k}) = \frac{1}{2} [\tilde{E}_f + \varepsilon_d(\mathbf{k}) \pm ([\tilde{E}_f - \varepsilon_d(\mathbf{k})]^2 + 4|\tilde{V}(\mathbf{k})|^2)^{1/2}]. \tag{1}$$

References

1. Anderson PW. Localized Magnetic States in Metals. *Phys Rev B* 1961;**124**:41.
2. Bianchi A, Movshovich R, Caban C, Pagluso PG, Sarrao JL. A possible Fulde-Ferrel-Larkin-Ovchinnikov superconducting state in Ce Co In5. *Phys Rev Lett* 2003;**91**:187004.
3. Callaway J, Chen DP, Kanhere DG, Misra PK. Cluster Simulation of the Lattice Anderson Model. *Phys Rev B* 1988;**38**:2583.
4. Demuer A, Sheikin I, Braithwaite D, Fak B, Huxley A, Raymond S, Flouquet J. *J. Magn. Matter* 2001;**17**:226.
5. Coleman P. *Physica B* 2006;**378–380**:1160.
6. Doniach S. The Kondo lattice and weak antiferromagnetism. *Physica B* 1977;**91**:231.
7. Fulde P, Ferrell RA. Superconductivity in Strong Spin-Exchange Field. *Phys Rev A* 1964;**135**:550.
8. Griveau J-C, Boulet P, Collineau E, Wastin F, Rebizant J. Pressure effect on PuMGd5(M=Co, Rh, Zr). *Physica B* 2005;**359–361**:1093.
9. Hewson AC. *The Kondo problem in heavy fermions*. Cambridge: Cambridge University Press; 1993.
10. Holmes AT, Jaccard D, Miyake K. Signatures of Valence Fluctuations in $CeCu_2Si_2$ under high pressure. *Phys Rev B* 2004;**69**:024508.
11. Kadowaki K, Woods SB. A universal relationship of the resistivity and specific heat of heavy-Fermion compounds. *Solid State Commun* 1986;**58**:507.

12. Kasuya T. A Theory of Metallic Ferro- and Antiferromagnetism in Zener's model. *Prog Theor Phys (Kyoto)* 1956;**16**:45.
13. Larkin AI, Ovchinnikov YN. Inhomogeneous state of superconductor. *Sov Phys JETP* 1965;**20**:762.
14. Luttinger JW. Fermi Surface and Some Simple Equilibrium Properties of a system of Interacting Fermions. *Phys Rev* 1960;**119**:1153.
15. Measson M-A, Brison JP, Seyfarth G, Braithwaite D, Lapertat G, Salce B, et al. Superconductivity of the filled skutterdite-PrOs4Sb12. *Physica* 2005;**359–361**:827.
16. Misra PK. *Heavy-fermion systems*. Amsterdam: Elsevier; 2008.
17. Misra PK, Kanhere DG, Callaway J. Periodic Anderson Model for four-site clusters. *Phys Rev B* 1987;**35**:5013.
18. Ott HR. Heavy-electrons and non-Fermi liquids, the early times. *Physica B* 2006;**378–380**:1.
19. Ott HR, Rudigier H, Delsing P, Fisk Z. UBe3:An unconventional Actinide Superconductor. *Phys Rev Lett* 1983;**50**:1595.
20. Riseborough PS. Heavy fermion semiconductors. *Adv Phys* 2000;**49**:257.
21. Ruderman MA, Kittel C. Indirect Exchange Coupling of Nuclear Magnetic Moments by Conduction Electrons. *Phys Rev* 1954;**96**:99.
22. Sarrao JL, Morales LA, Thompson JD, Scole BL, Stewart GR, Wastin F, et al. Plutonium-based Superconductivity with a transition temperature above 18K. *Nature* 2002;**420**:297.
23. Sarrao JL, Brauer ED, Morales LA, Thompson JD. Structural tuning and anisotropy in PuCoGa5. *Physica B* 2005;**359–361**:1144.
24. Schrieffer JR, Wolff PA. Rekation between the Anderson and Kondo Hamiltonian. *Phys Rev* 1966;**149**:491.
25. Senthil T, Sachdev S, Vojta M. Quantum phase transition out of the heavy Fermi liquid. *Physica* 2005;**359–361**:9.
26. Senthil T, Sachdev S, Vojta M. Fractionalized Fermi liquids. *Phys Rev Lett* 2003;**90**:216403.
27. Senthil T, Vojta M, Sachdev S. Weak magnetism and non-Fermi liquids near heavy-fermion critical points. *Phys Rev B* 2004;**69**:035111.
28. Smith JL, Si Q. Spatial correlations in dynamical mean-field theory. *Phys Rev B* 2000;**61**:5184.
29. Steglich F, Aarts J, Bredl CD, Lieke W, Meschede D, Franz W, et al. Superconductivity in the Presence of Strong Pauli Paramagnetism: $CeCu_2Si_2$. *Phys Rev Lett* 1979;**43**:1892.
30. Stewart GR. Heavy-fermion systems. Possibility of Coexistence of Bulk Supercon. *Rev Mod Phys* 1984;**56**:755.
31. Stewart GR, Rudigier H, Delsing P, Fisk Z. Possibility of Coexistence of Bulk Supercon. *Phys Rev Lett* 1984;**52**:679.
32. Varma CM. Mixed-Valence Compounds. *Rev Mod Phys* 1976;**48**:219.
33. Wachter P. Similarities between Cu and Pu containing "high-Tc Superconductor." *Physica C* 2007;**453**:1.
34. Wasrtin F, Boule P, Rebizant J, Collineau E, Lander GH. Advances in the preparation and characterization of transuranium systems. *J. Phys. Condens. Matter* 2003;**15**:S2279.
35. Wilson KG. The renormalization group: Critical phenomena and the Kondo problem. *Rev Mod Phys* 1975;**47**:773.
36. Yosida K. Magnetic Properties of Cu-Mn Alloys. *Phys Rev* 1957;**106**:893.